Electronic Supplementary Material (ESI) for New Journal of Chemistry.

Supplementary information

Synthesis, structures and mechanistic pathways of anticancer activity of palladium(II) complexes with indole-3-carbaldehyde thiosemicarbazones

Jebiti Haribabu,[a] Manoharan Muthu Tamizh,[b] Chandrasekar Balachandran,[c] Yuvaraj Arun,[d] Nattamai S. P. Bhuvanesh,[e] Akira Endo,[f] and Ramasamy Karvembu[a]*

[a] *Department of Chemistry, National Institute of Technology, Tiruchirappalli - 620015, India. E-mail address: kar@nitt.edu (R. Karvembu); Fax: +91 431 2500133; Tel: +91 431 2503631*

[b] *Department of Chemistry, Siddha Central Research Institute, Central Council for Research in Siddha, Arumbakkam, Chennai- 600 106, India*

[c] *Division of Natural Drug Discovery, Institute of Natural Medicine, University of Toyama, 2630 Sugitani, Toyama 930-0194, Japan*

[d] *Organic Chemistry Division, CSIR-Central Leather Research Institute, Chennai - 600020, India*

[e] *Department of Chemistry, Texas A & M University, College Station, TX 77842, USA*

[f] *Department of Materials and Life Sciences, Sophia University, 7-1 Kioicho, Chiyoda-ku, Tokyo 102-8554, Japan*

Hydrodynamic (viscosity) studies

A hydrodynamic method such as viscosity measurement is sensitive to length changes and offers a clear clue regarding the mode of interaction. A classical intercalator lengthens DNA helix, which is due to the separation in the DNA base pairs when the compound slides in between and as a result of which the viscosity increases. In contrast, a partial, non-classical intercalation of molecules could bend (or kink) the DNA helix, reducing its length and, concomitantly, its viscosity. The complexes which bind with DNA grooves cause less noticeable or no variation in the viscosity.[1,2] The viscosity of DNA increased with increasing the concentration of the complexes and the resultant graph is displayed in Figure S41. The results revealed the binding of the complexes with DNA *via* intercalation. The ability of the complexes to increase the viscosity of DNA followed the order **4 > 5 > 3 > 1 > 2**.

Circular dichroism (CD) studies

The interaction of the palladium(II) complexes with CT DNA was further confirmed by CD technique. CD spectrum of DNA showed two bands at 276 (positive band) and 245 nm (negative band), arising due to base stacking and helicity, which are characteristic of DNA in the right-handed B form.[3] Groove binding and electrostatic interaction of small molecules with DNA show a very little or no change in the bands while intercalation changes the intensity of both the bands.[4] On addition of the palladium(II) complexes (**1**-**5**) to CT DNA, an increase in positive and a decrease in negative ellipticity with a small red shift were observed. These changes in the CD spectrum of DNA indicated strong conformational disturbances induced by complexes **1**-**5**.[5] It was observed that complex **4** showed significant changes in the CD spectrum of DNA than the other complexes (Figure S42). Furthermore, the decrease in negative band is probably due to the unwinding of DNA helix upon interaction with the palladium(II) complexes and then it is transformed into A-DNA form.[6,7]

Synchronous fluorescence spectra

Synchronous fluorescence spectroscopy can give information about the conformational changes in the protein molecular environment in the vicinity of the fluorophore functional groups.[8] The fluorescence of BSA is due to tyrosine and tryptophan residues. According to

Miller,[9] the difference between excitation and emission wavelengths ($\Delta\lambda = \lambda_{emi} - \lambda_{exc}$) reflects the spectra of different nature of chromophores. The small $\Delta\lambda$ value (15 nm) is characteristic of tyrosine residue and large $\Delta\lambda$ value (60 nm) is characteristic of tryptophan residue.[10] On addition of palladium(II) complexes **1**-**5**, the fluorescence intensity of tyrosine residue at 304 nm decreased in the magnitude of 66.1, 62.7, 73.0, 69.5 and 75.2 % respectively, with no appreciable shift (Figure S44). Similarly, there was also a decrease in the intensity of tryptophan residue at 340 nm by 75.2, 70.9, 67.5, 79.2 and 80.6 % for palladium(II) complexes **1**-**5** respectively (Figure S45). The results showed that all the complexes affected the microenvironments of both tyrosine and tryptophan residues.

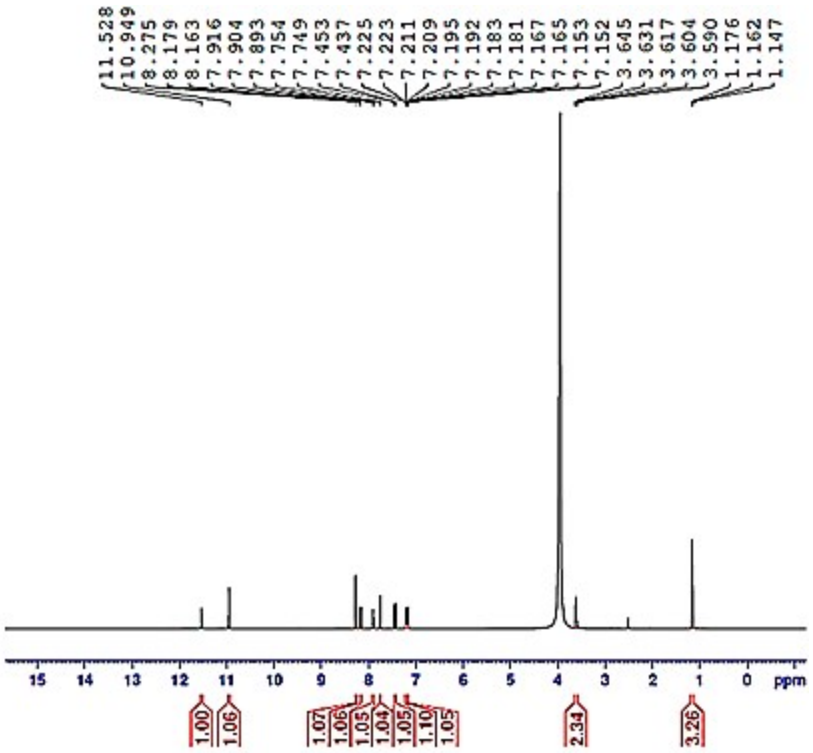

Figure S1. [1]H NMR spectrum of HL3.

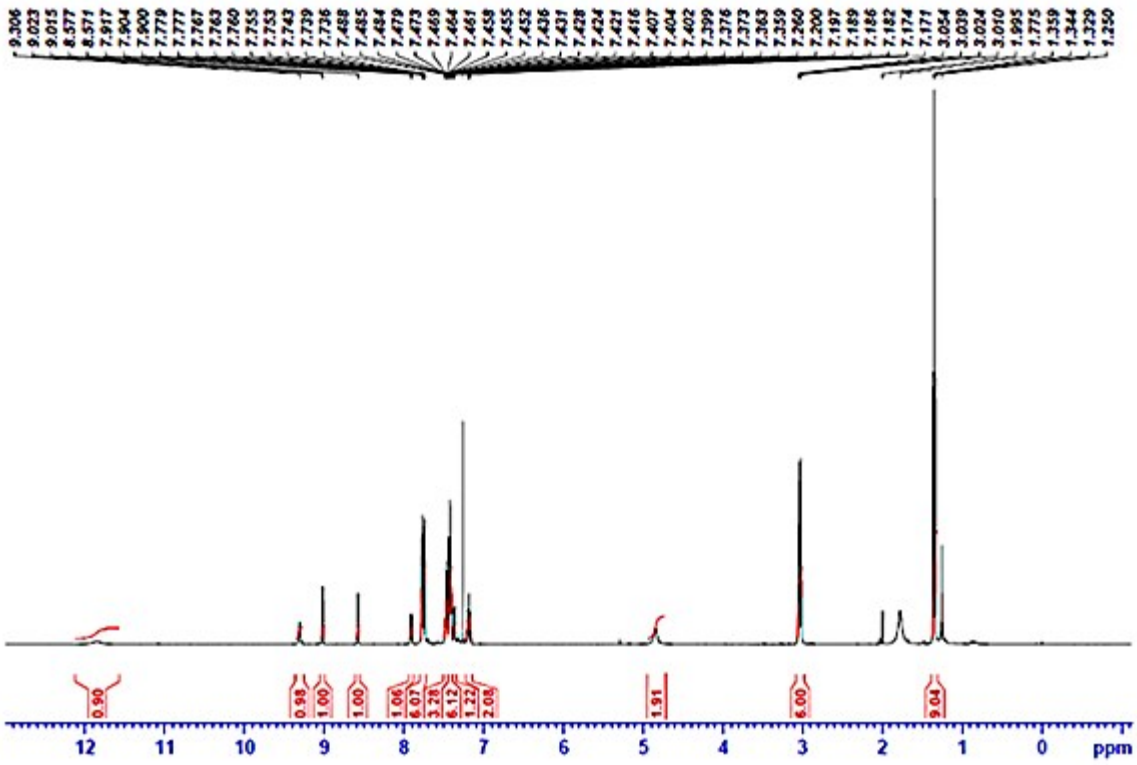

Figure S2. [1]H NMR spectrum of **1**.

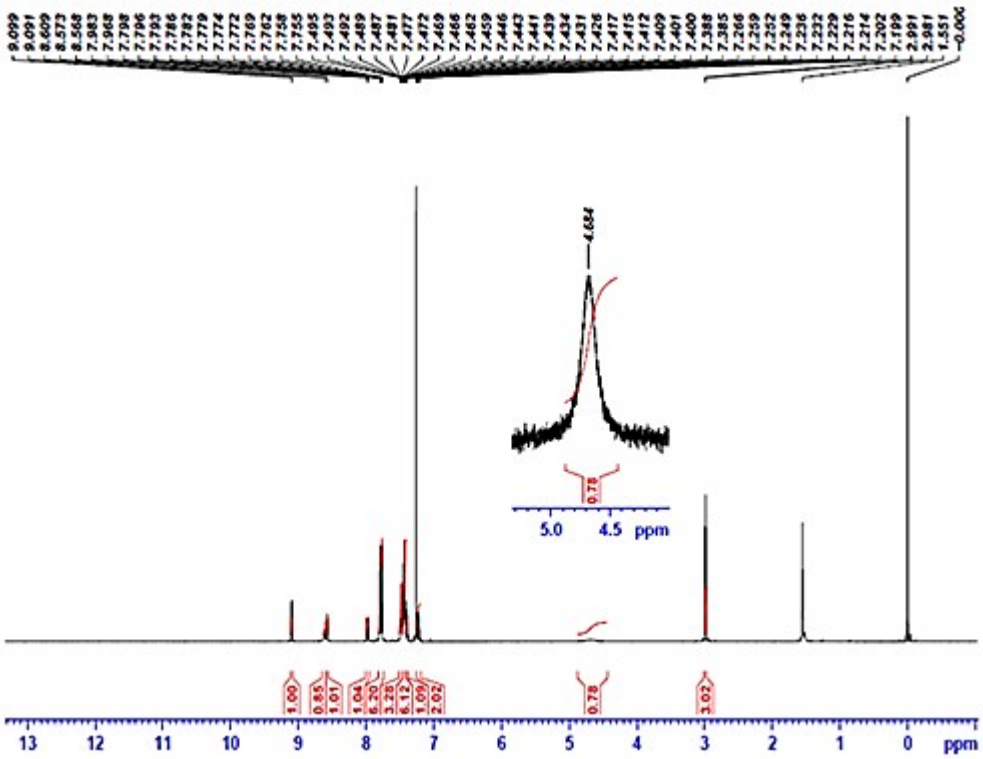

Figure S3. ^{1}H NMR spectrum of **2**.

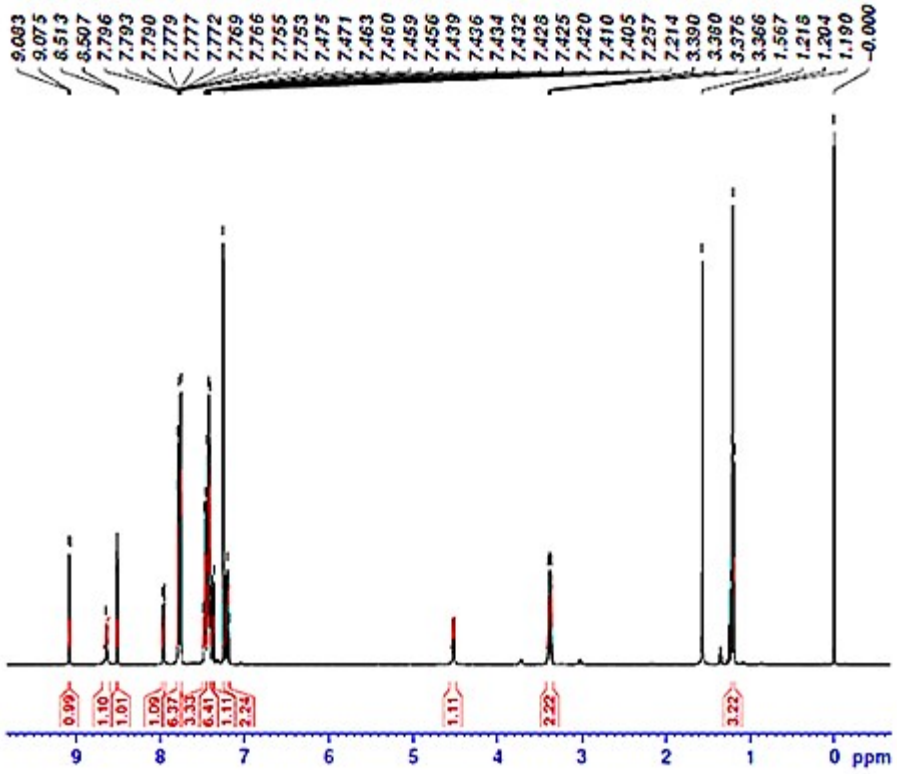

Figure S4. ^{1}H NMR spectrum of **3**.

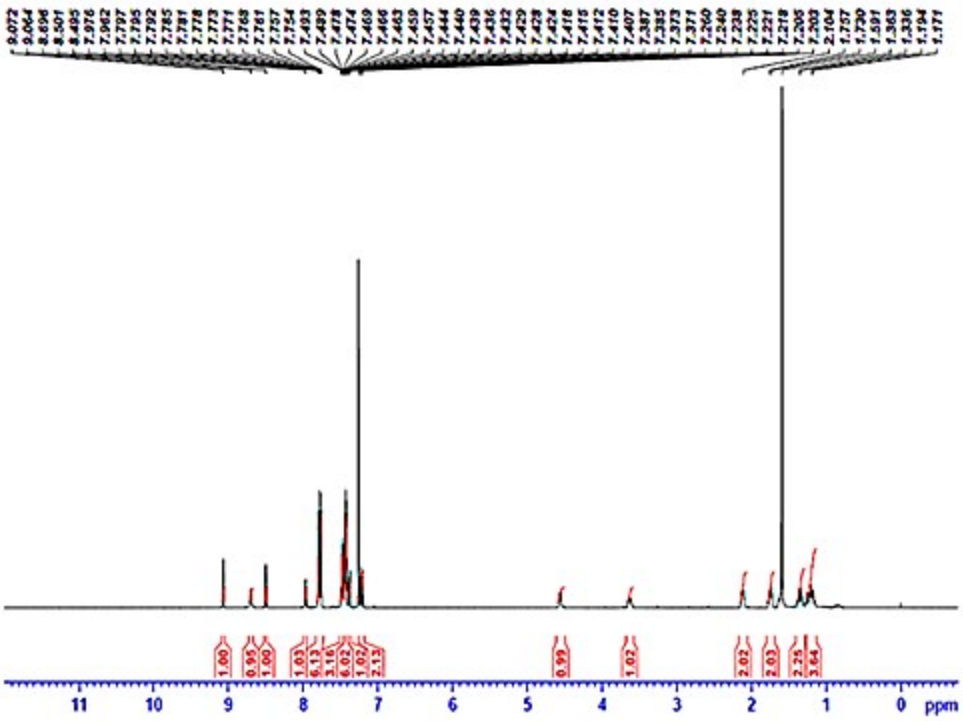

Figure S5. ^{1}H NMR spectrum of **4**.

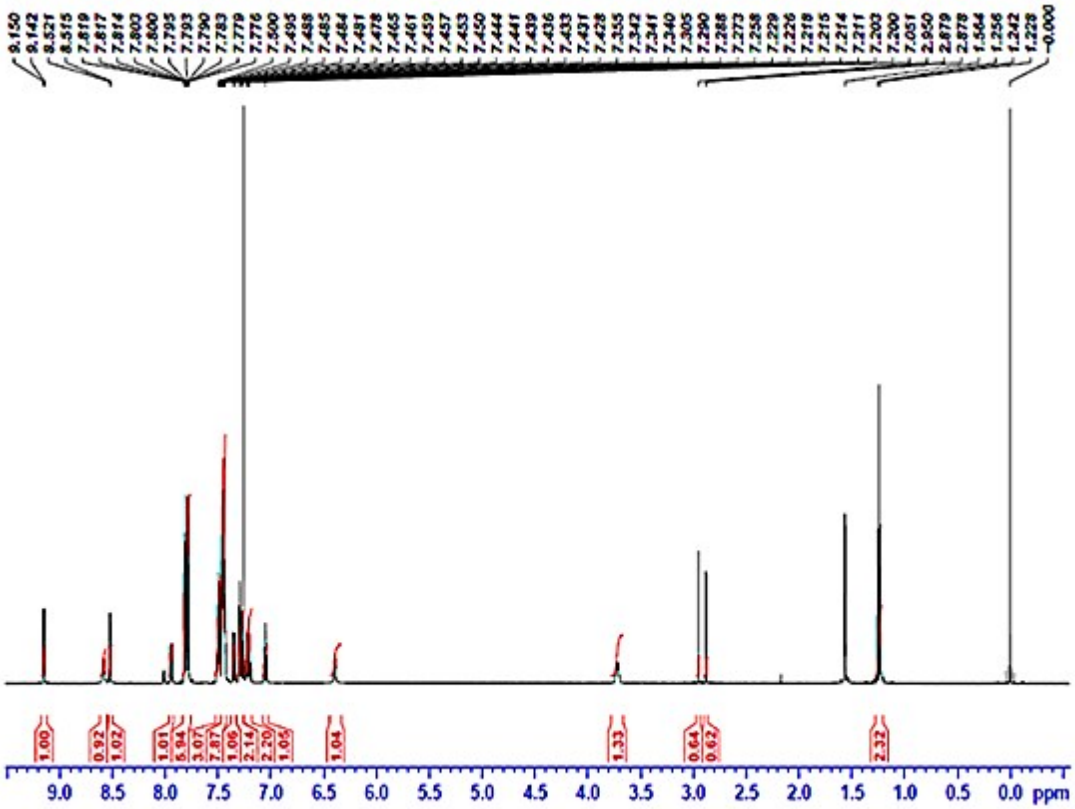

Figure S6. ^{1}H NMR spectrum of **5**.

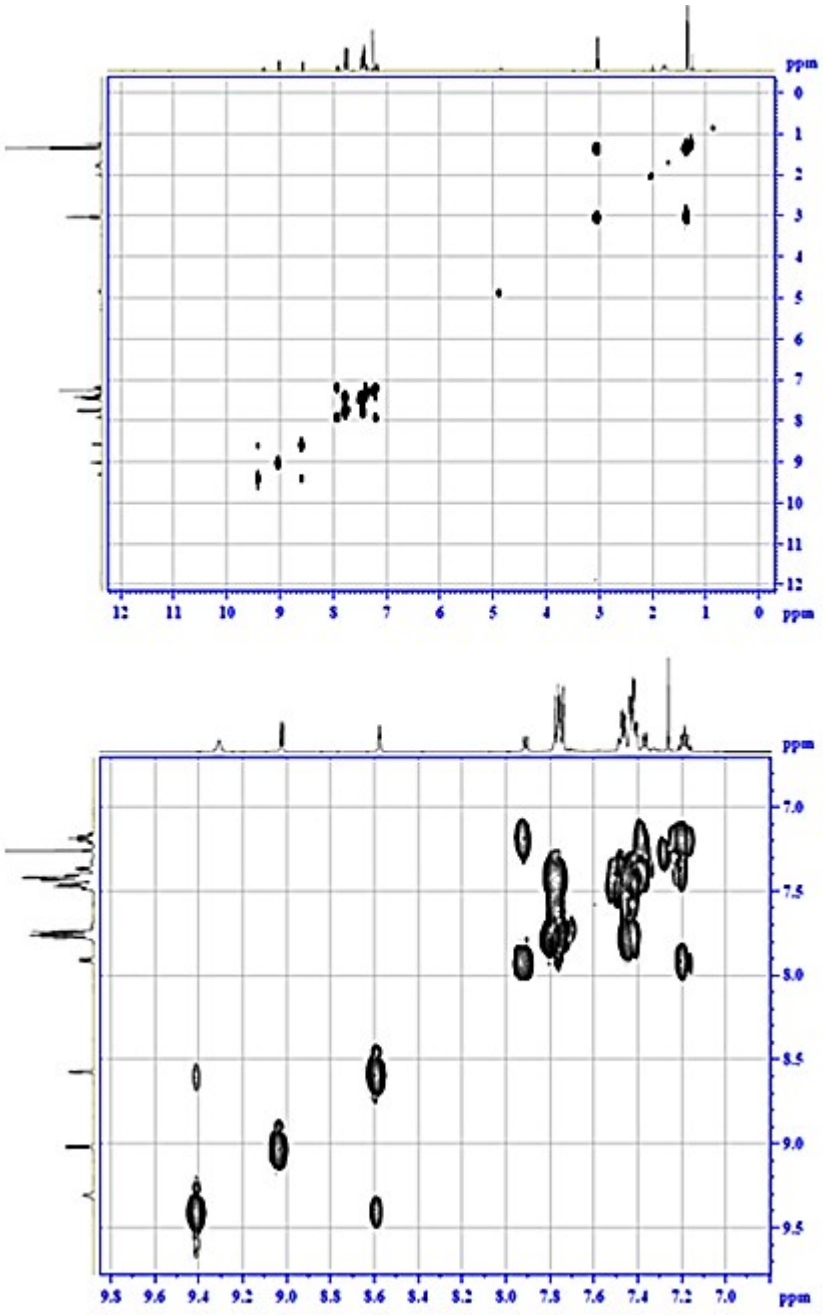

Figure S7. $^{1}H–^{1}H$ COSY and expansion of $^{1}H–^{1}H$ COSY spectrum of **1**.

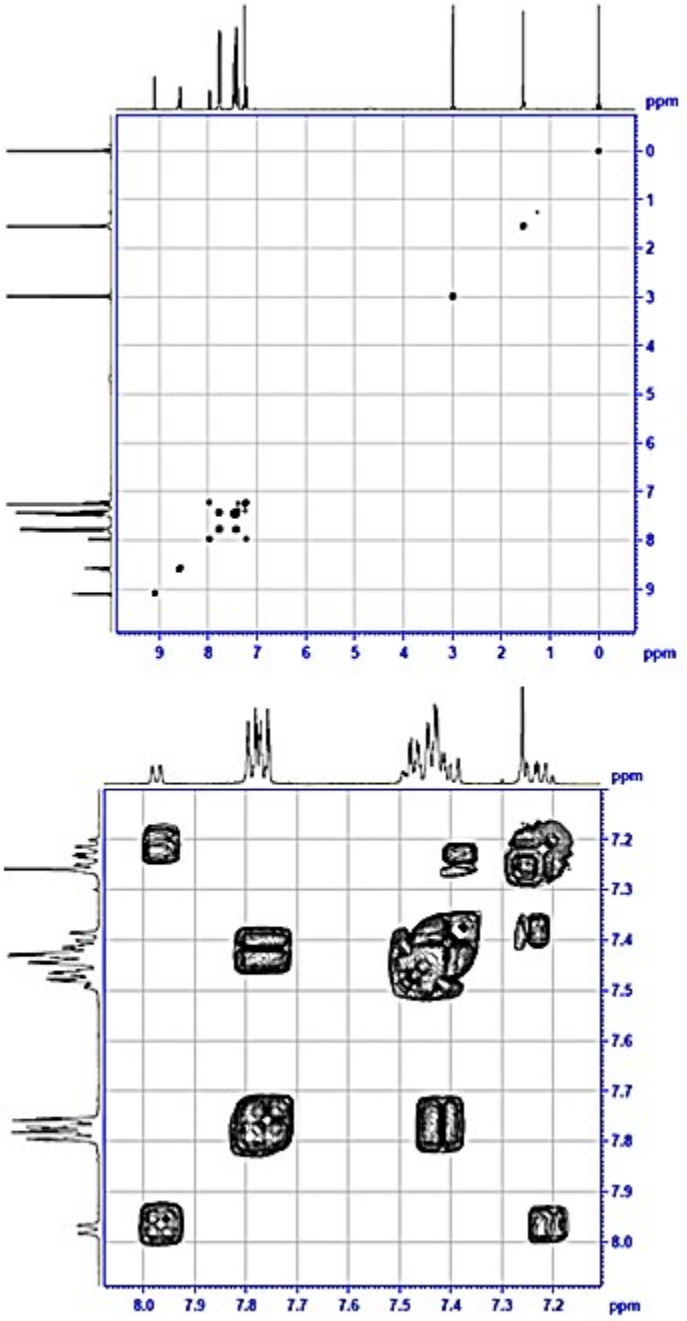

Figure S8. $^{1}H–^{1}H$ COSY and expansion of $^{1}H–^{1}H$ COSY spectrum of **2**.

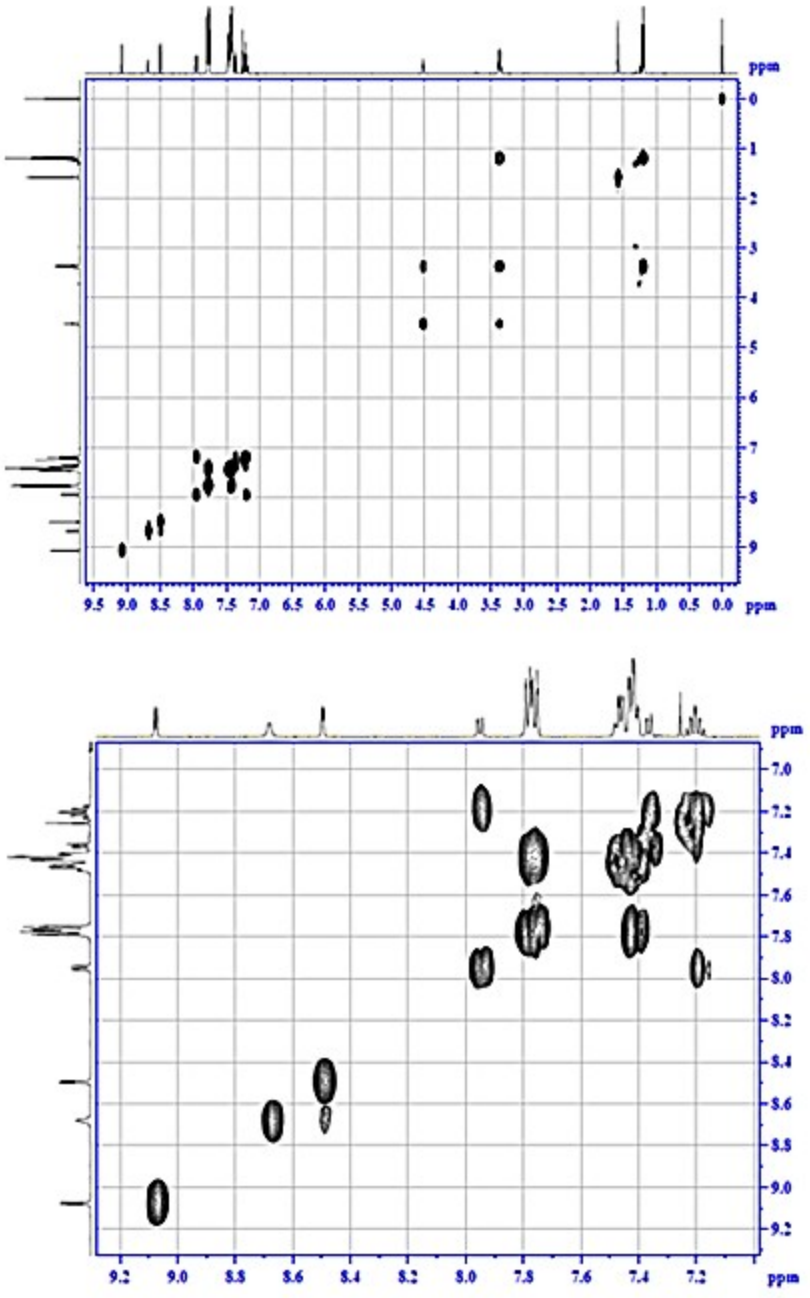

Figure S9. ^{1}H–^{1}H COSY and expansion of ^{1}H–^{1}H COSY spectrum of **3**.

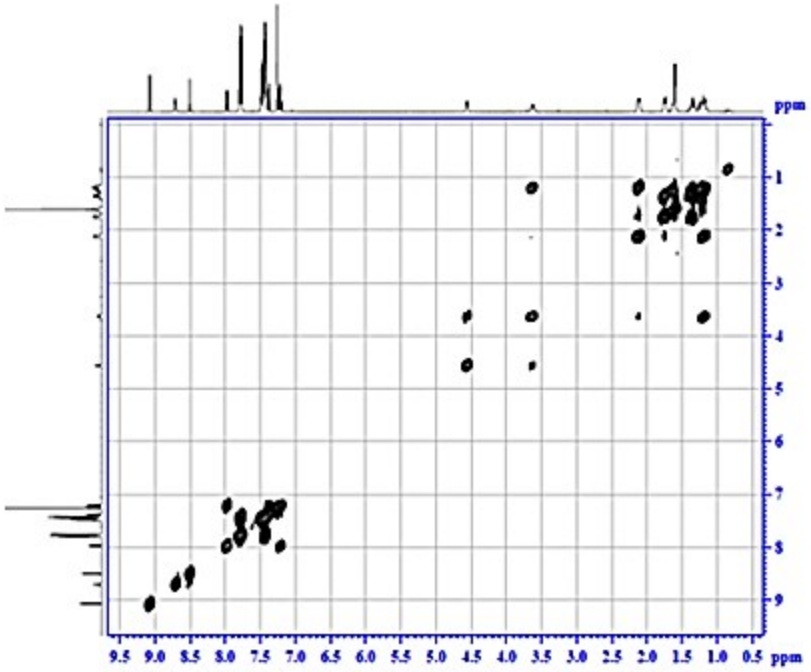
ppm
1
2
3
4
5
6
7
8
9
9.5 9.0 8.5 8.0 7.5 7.0 6.5 6.0 5.5 5.0 4.5 4.0 3.5 3.0 2.5 2.0 1.5 1.0 0.5 ppm

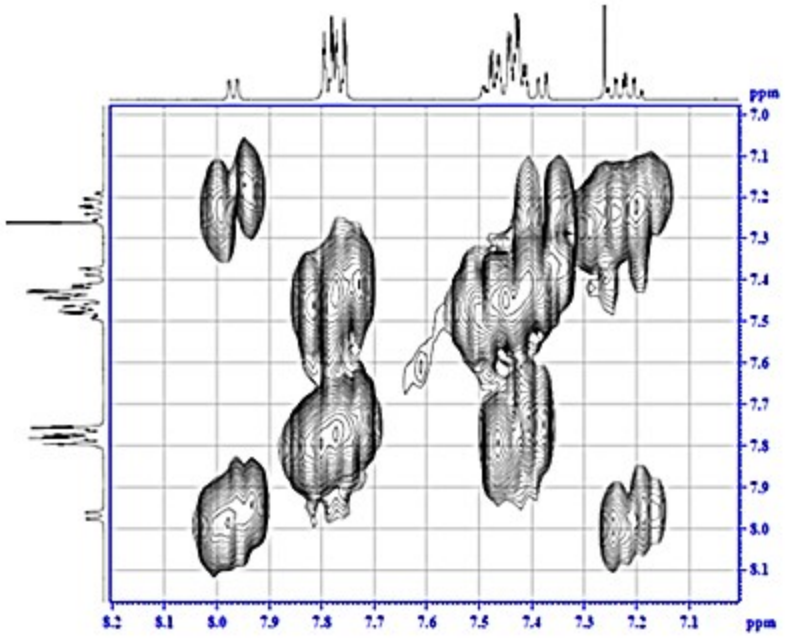
ppm
7.0
7.1
7.2
7.3
7.4
7.5
7.6
7.7
7.8
7.9
8.0
8.1
8.2 8.1 8.0 7.9 7.8 7.7 7.6 7.5 7.4 7.3 7.2 7.1 ppm

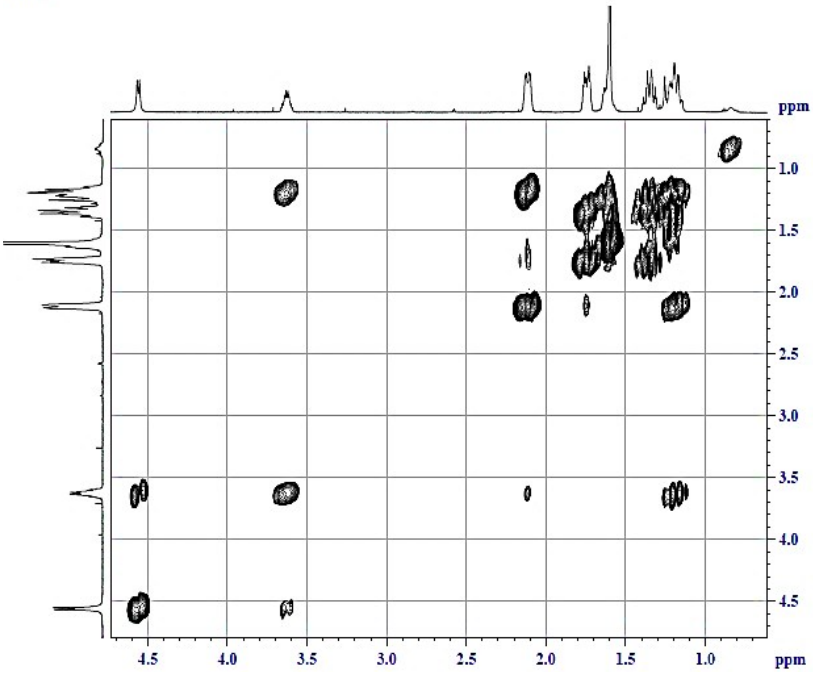

Figure S10. ^{1}H–^{1}H COSY and expansion of ^{1}H–^{1}H COSY spectrum of **4**.

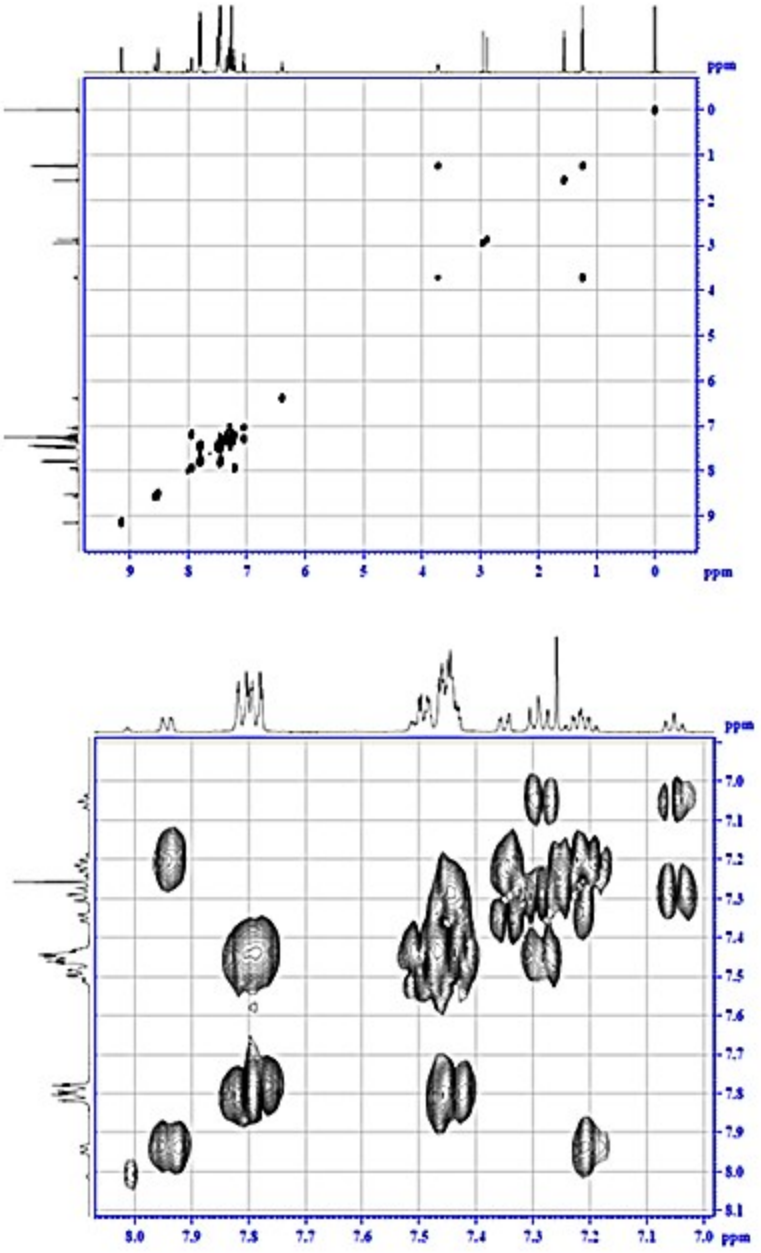

Figure S11. ^{1}H–^{1}H COSY and expansion of ^{1}H–^{1}H COSY spectrum of **5**.

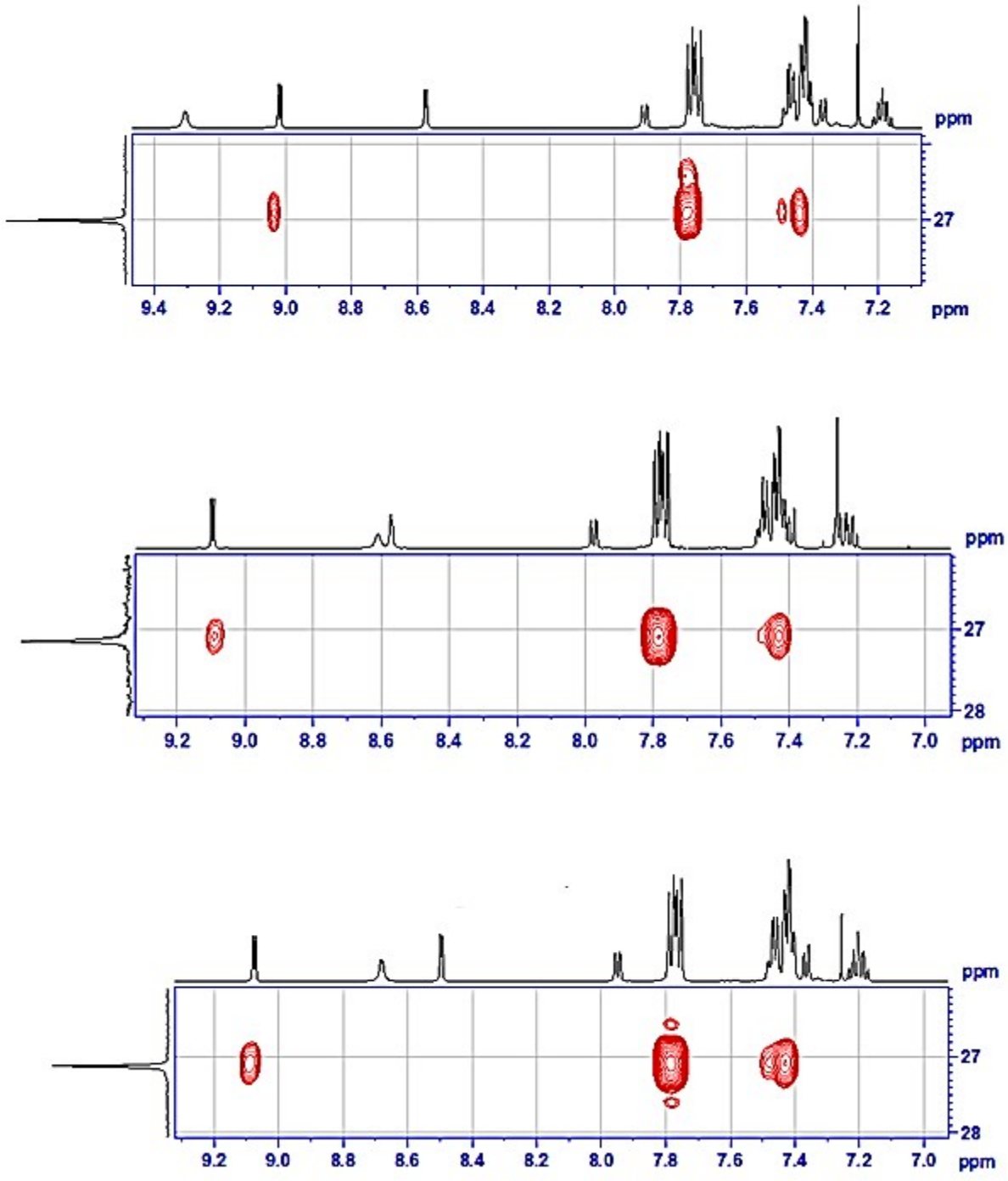

Figure S12. $^{1}H–^{11}P$ HMBC spectrum of **1-3**.

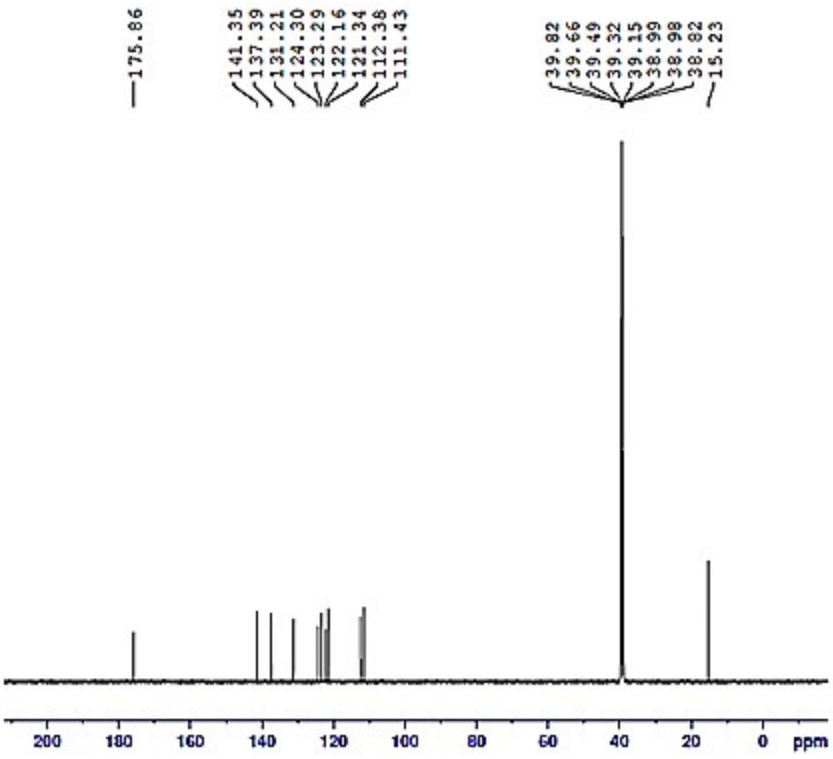

Figure S13. ^{13}C NMR spectrum of HL3.

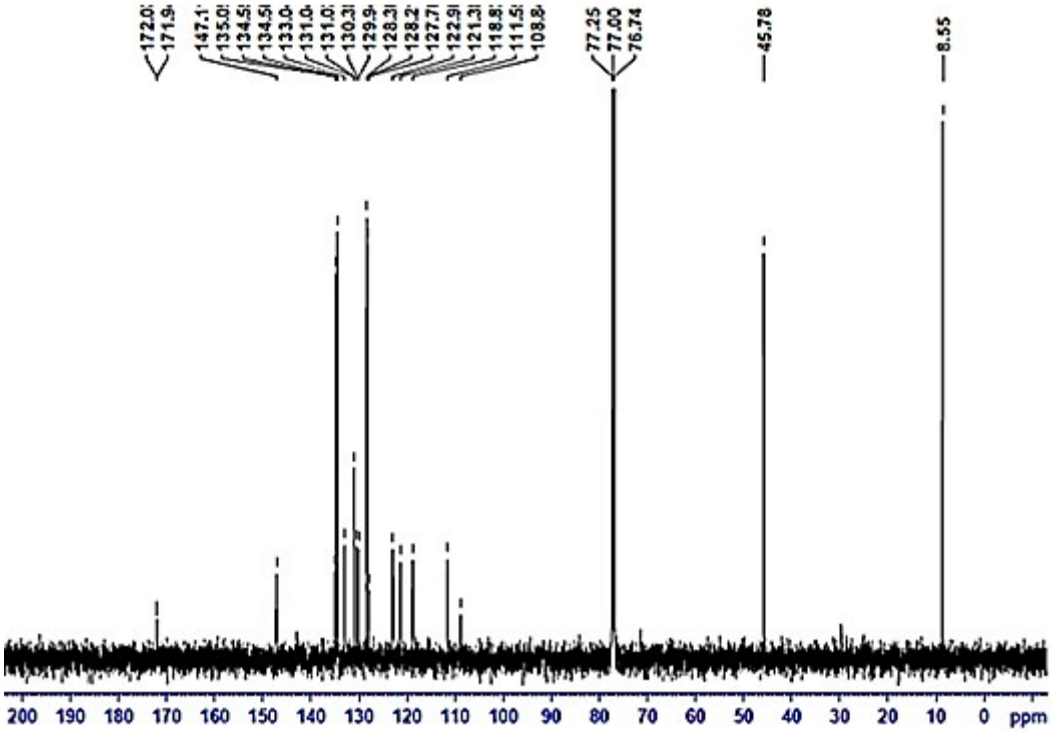

Figure S14. ^{13}C NMR spectrum of **1**.

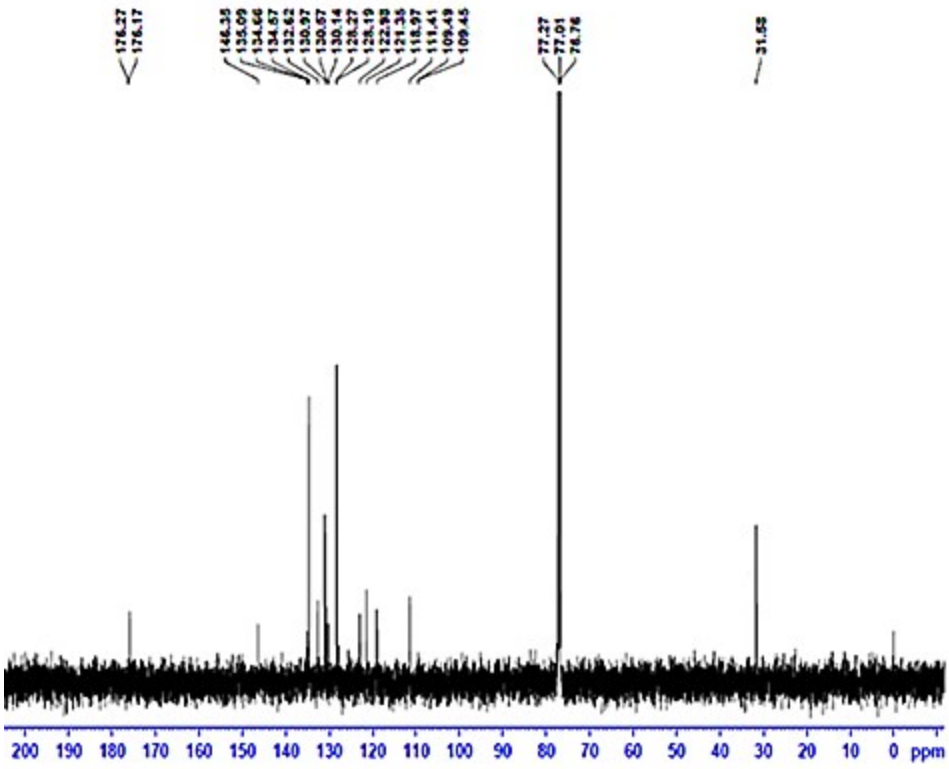

Figure S15. ^{13}C NMR spectrum of **2**.

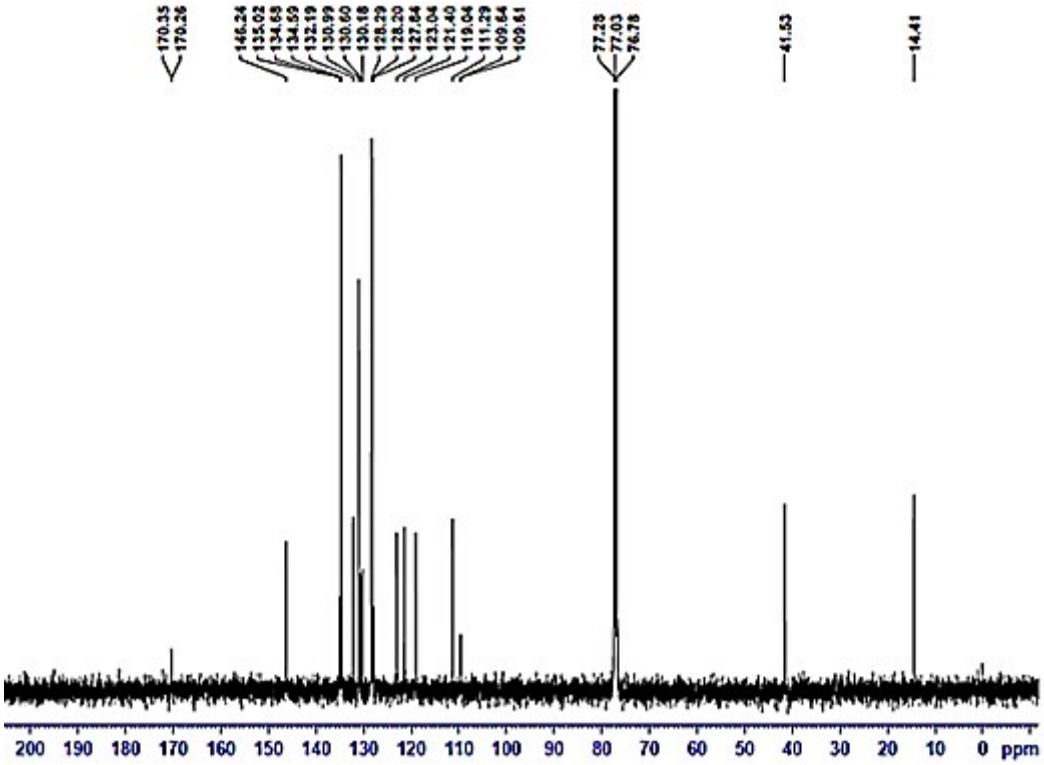

Figure S16. ^{13}C NMR spectrum of **3**.

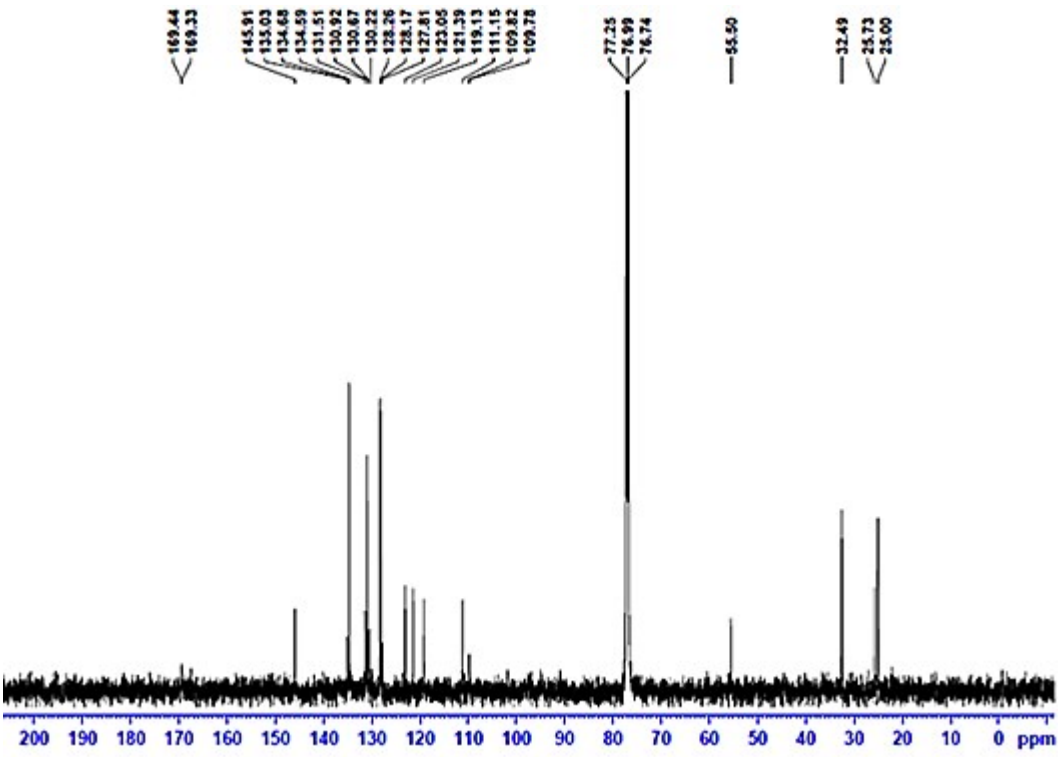

Figure S17. ^{13}C NMR spectrum of **4**.

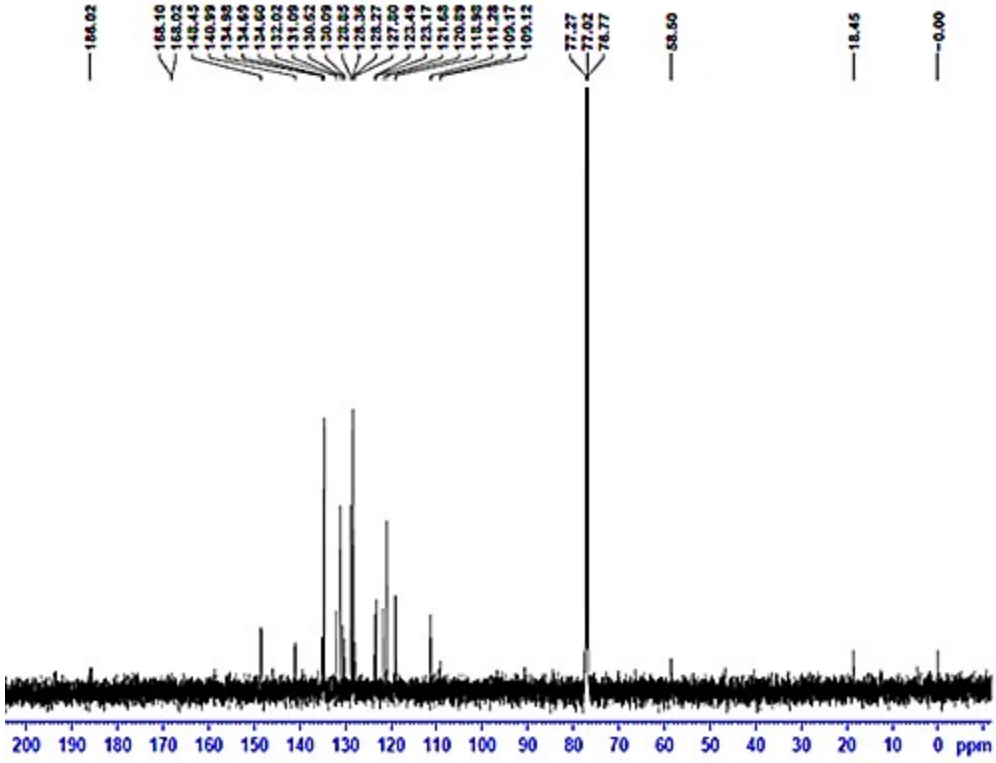

Figure S18. ^{13}C NMR spectrum of **5**.

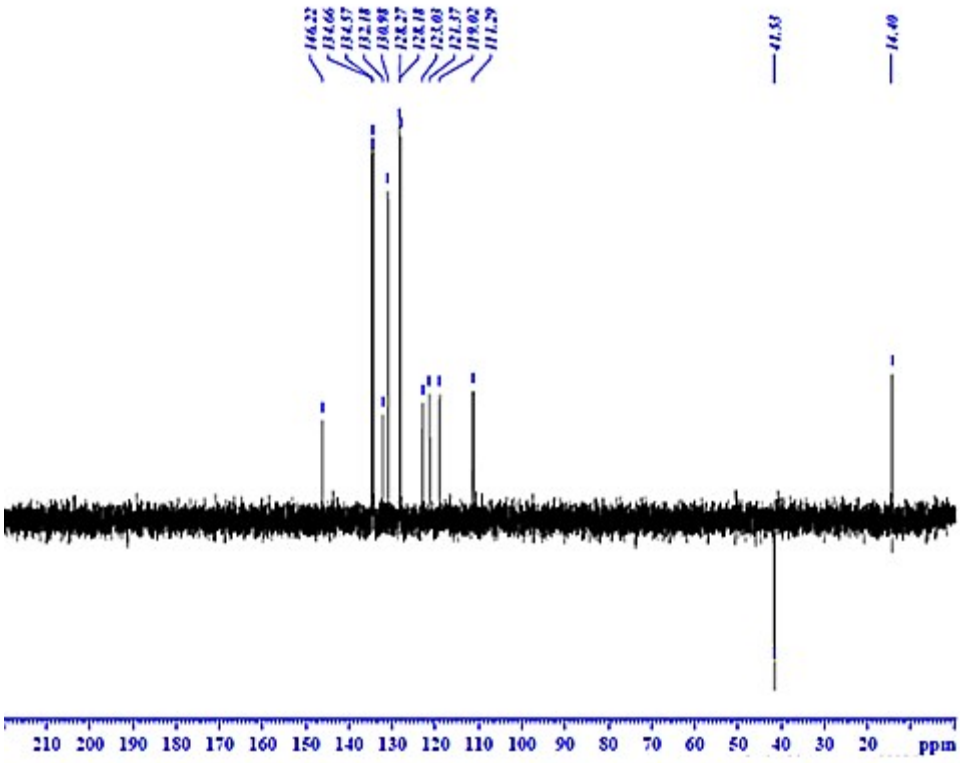

Figure S19. DEPT-135 NMR spectrum of **3**.

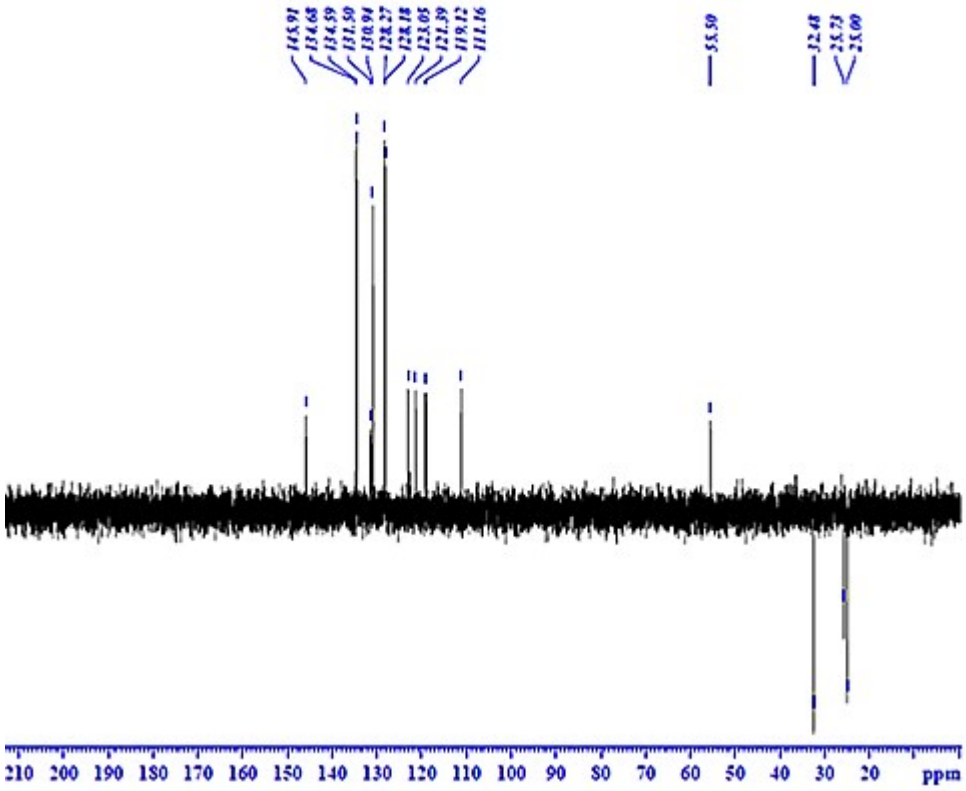

Figure S20. DEPT-135 NMR spectrum of **4**.

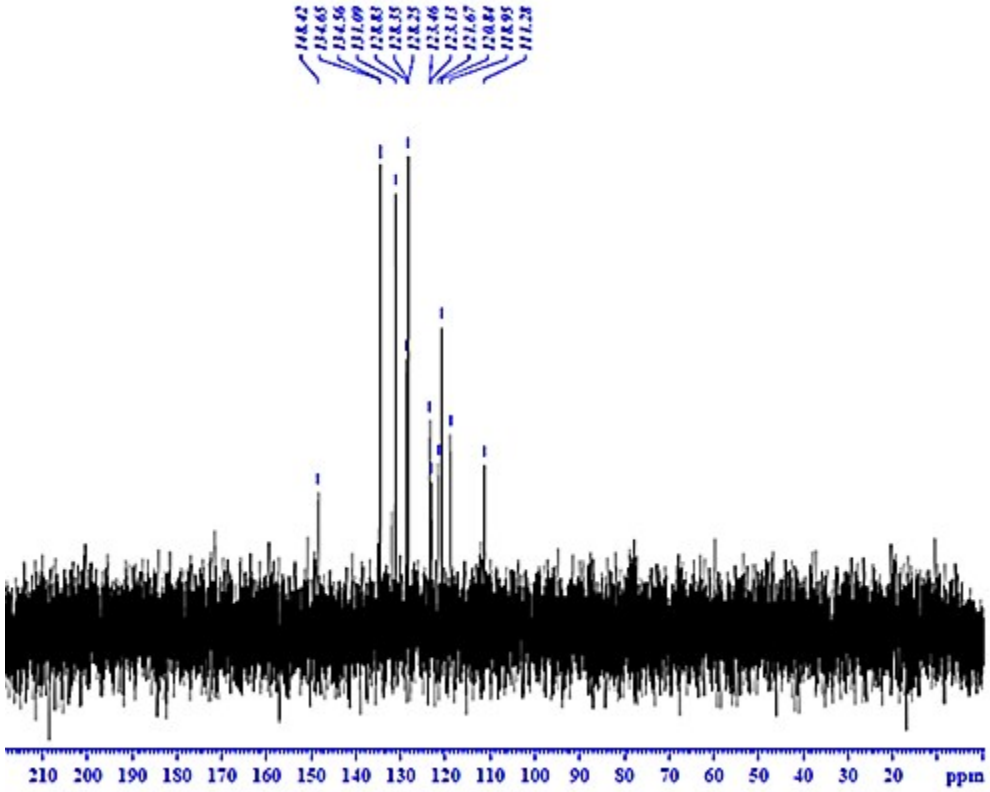

Figure S21. DEPT-135 NMR spectrum of **5**.

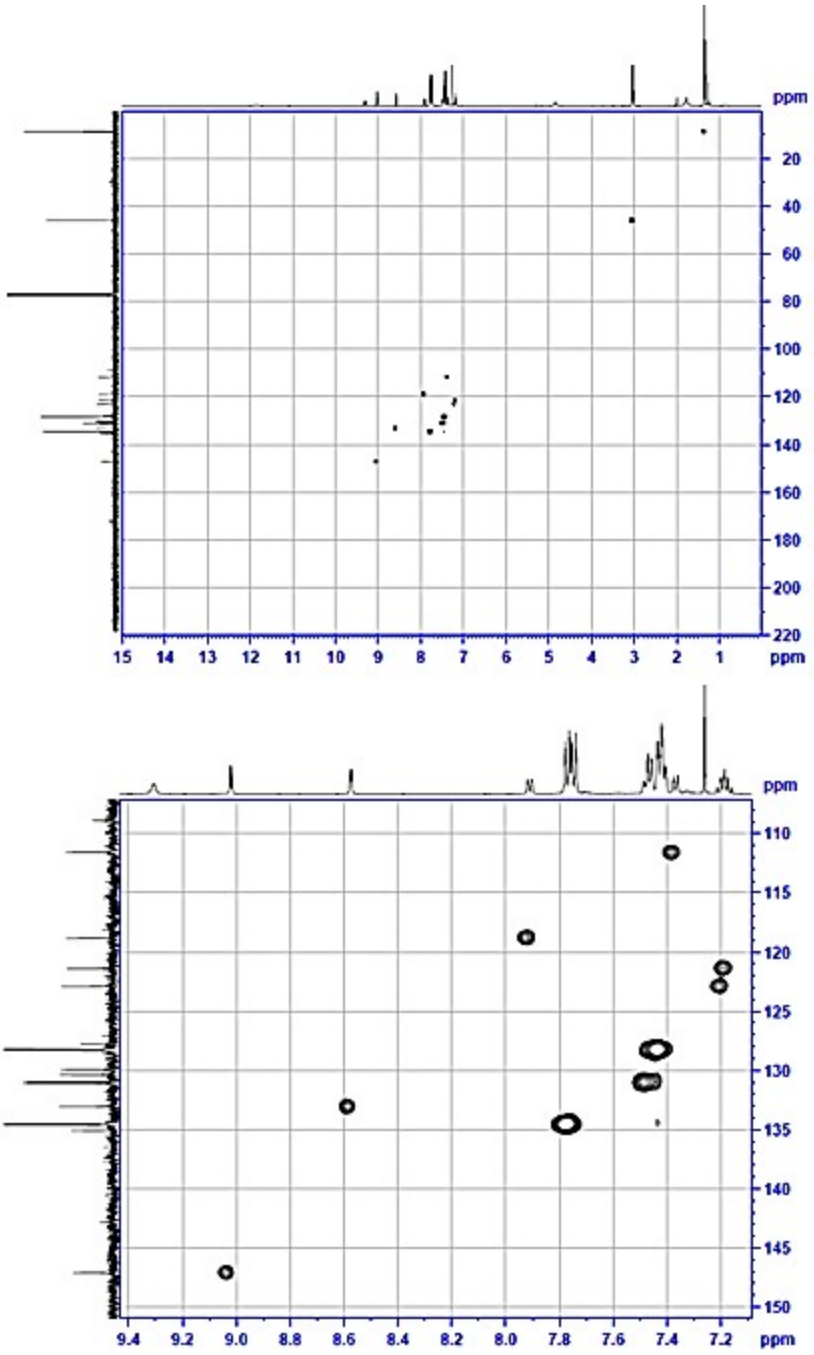

Figure S22. $^{1}H–^{13}C$ HSQC and expansion of $^{1}H–^{13}C$ HSQC spectrum of **1**.

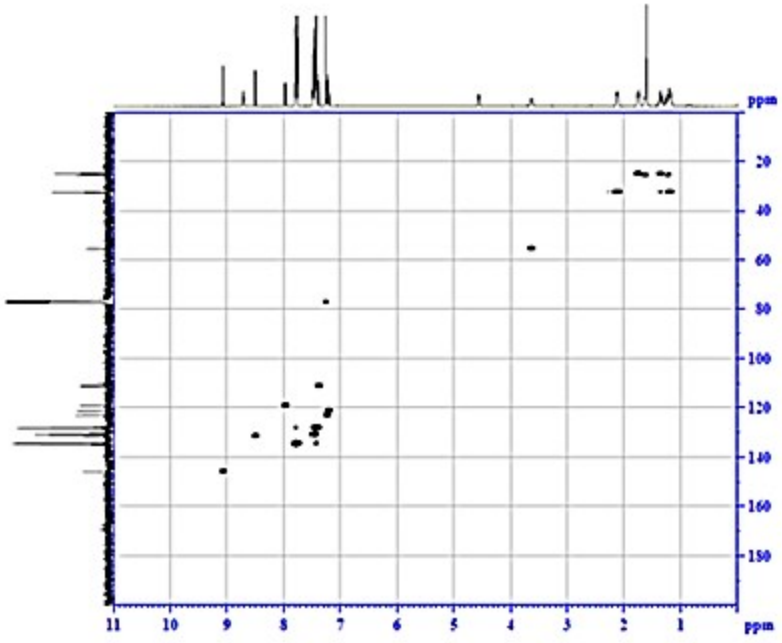
ppm
20
40
60
80
100
120
140
160
180
11
10
9
8
7
6
5
4
3
2
1
ppm

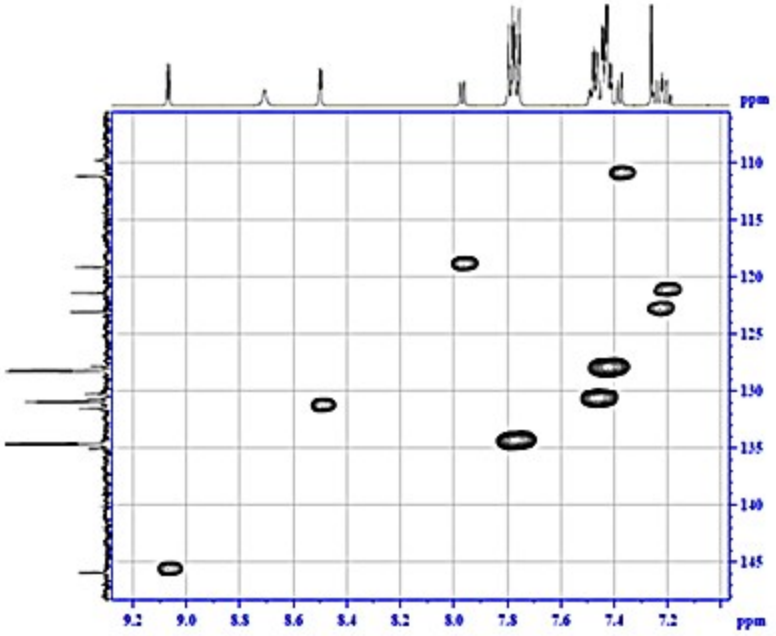
ppm
110
115
120
125
130
135
140
145
9.2
9.0
8.8
8.6
8.4
8.2
8.0
7.8
7.6
7.4
7.2
ppm

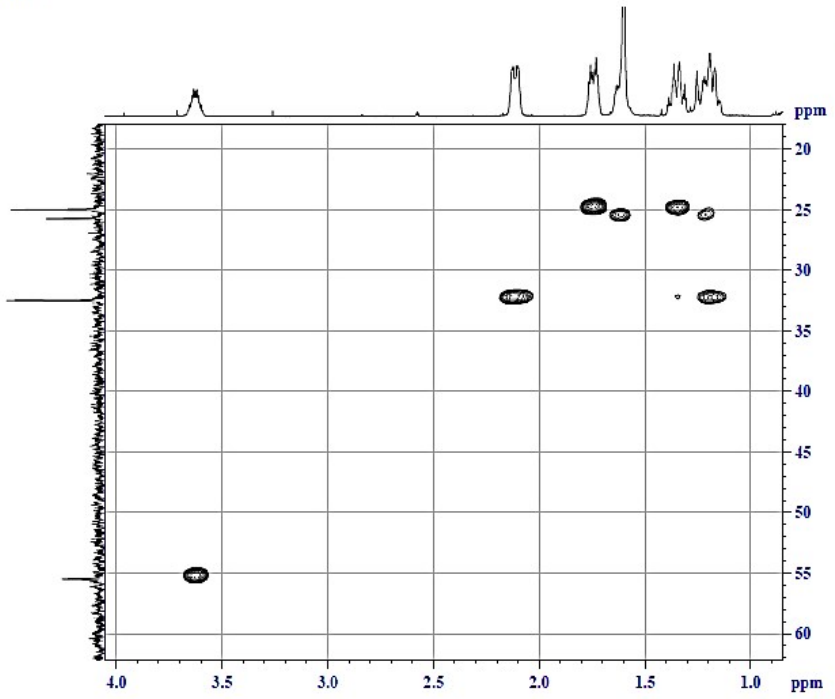

Figure S23. $^{1}H–^{13}C$ HSQC and expansion of $^{1}H–^{13}C$ HSQC spectrum of **4**.

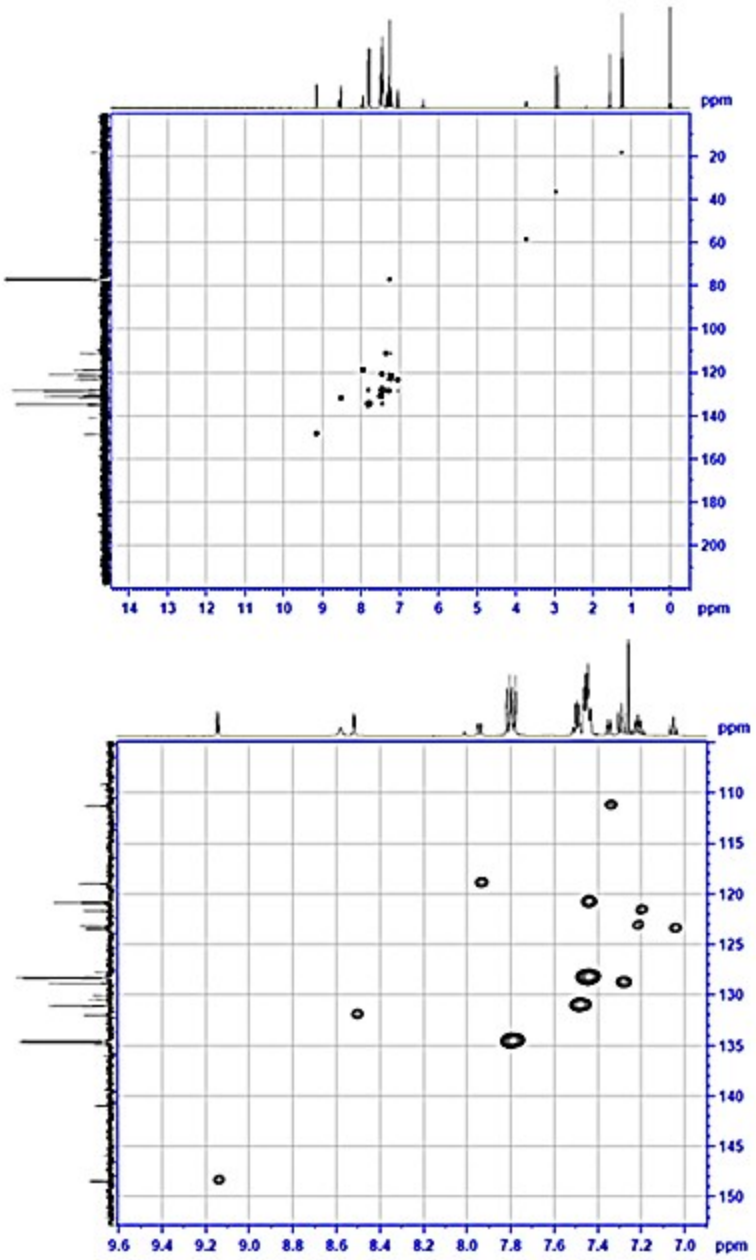

Figure S24. $^{1}H–^{13}C$ HSQC and expansion of $^{1}H–^{13}C$ HSQC spectrum of **5**.

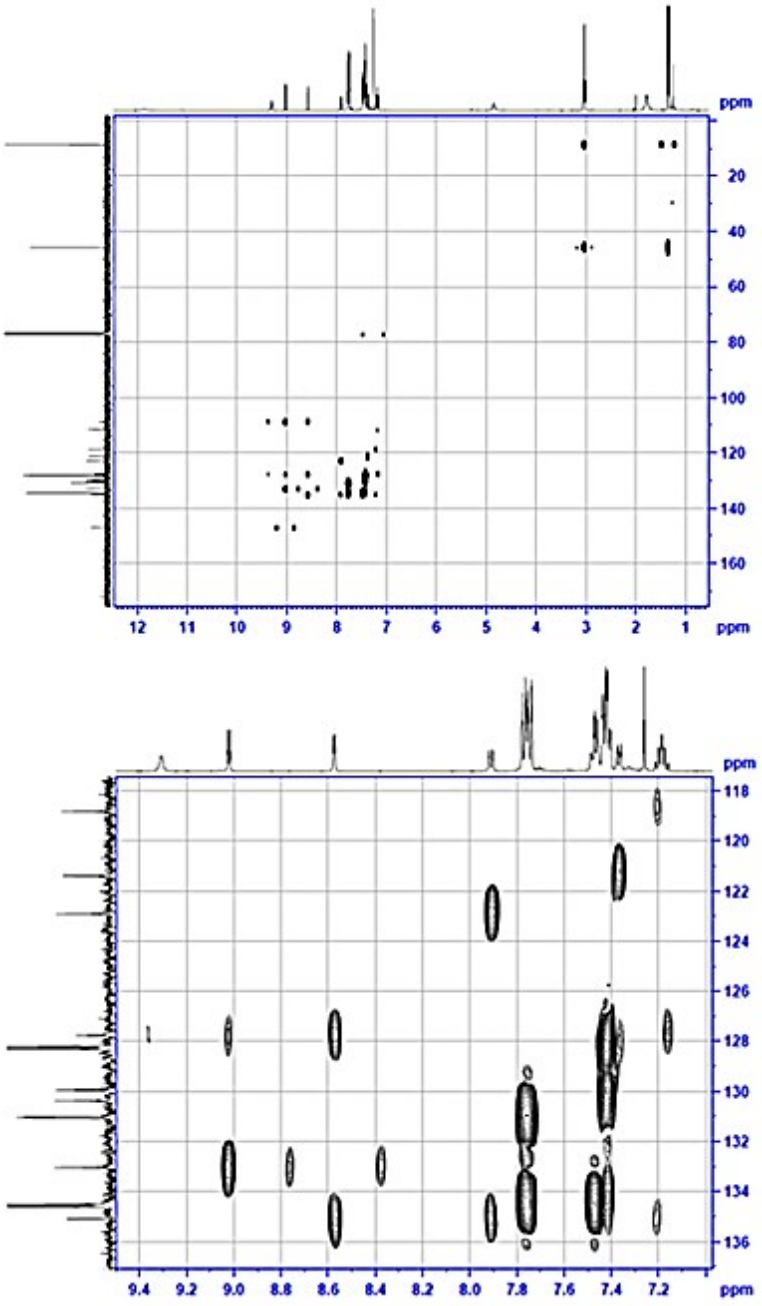

Figure S25. $^{1}H–^{13}C$ HMBC and expansion of $^{1}H–^{13}C$ HMBC spectrum of **1**.

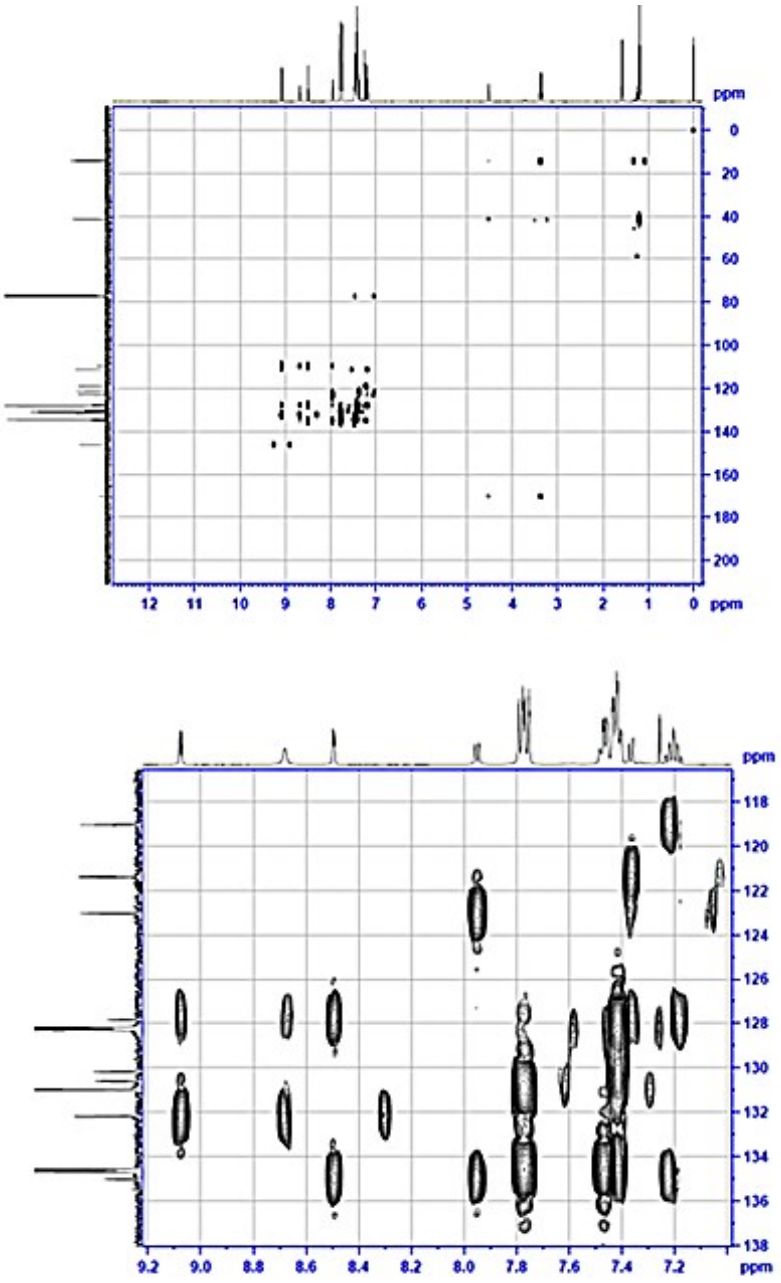

Figure S26. $^{1}H–^{13}C$ HMBC and expansion of $^{1}H–^{13}C$ HMBC spectrum of **3**.

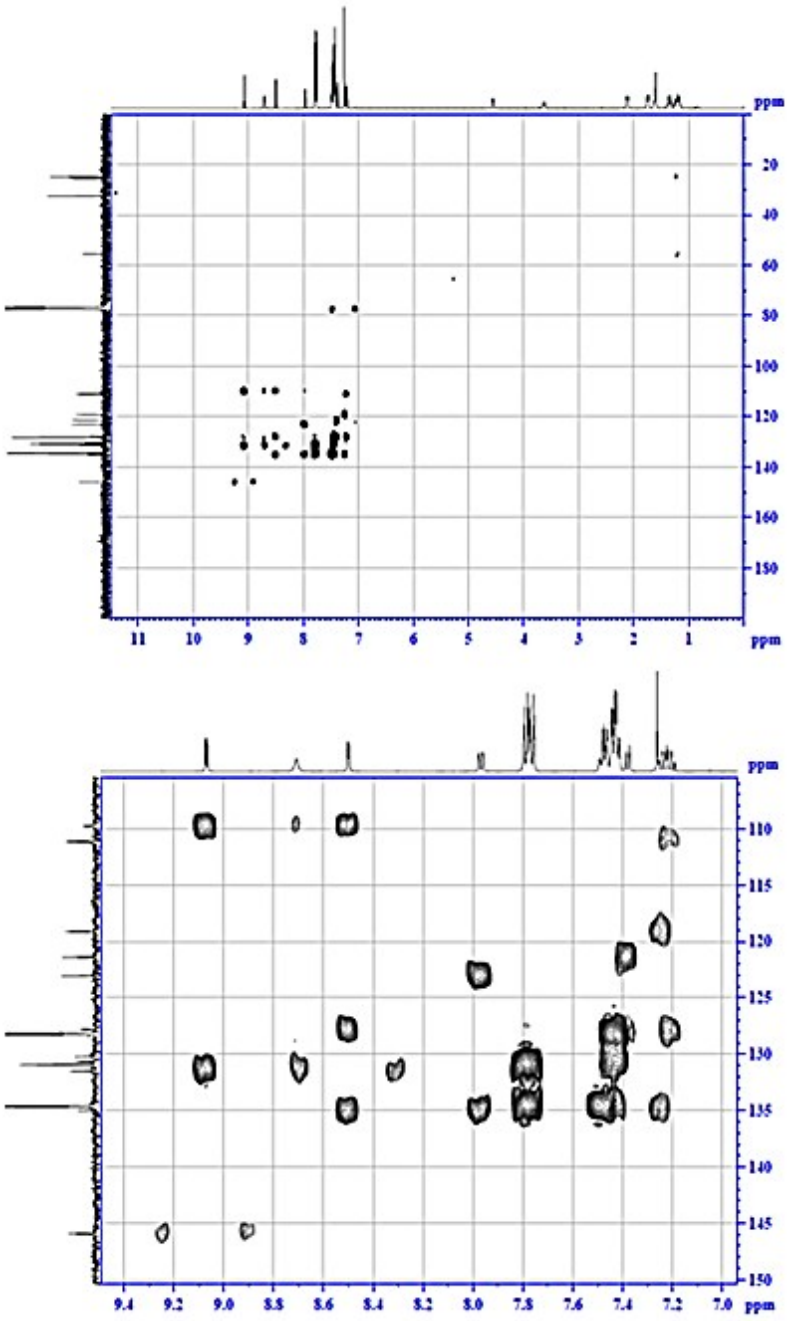

Figure S27. $^{1}H–^{13}C$ HMBC and expansion of $^{1}H–^{13}C$ HMBC spectrum of **4**.

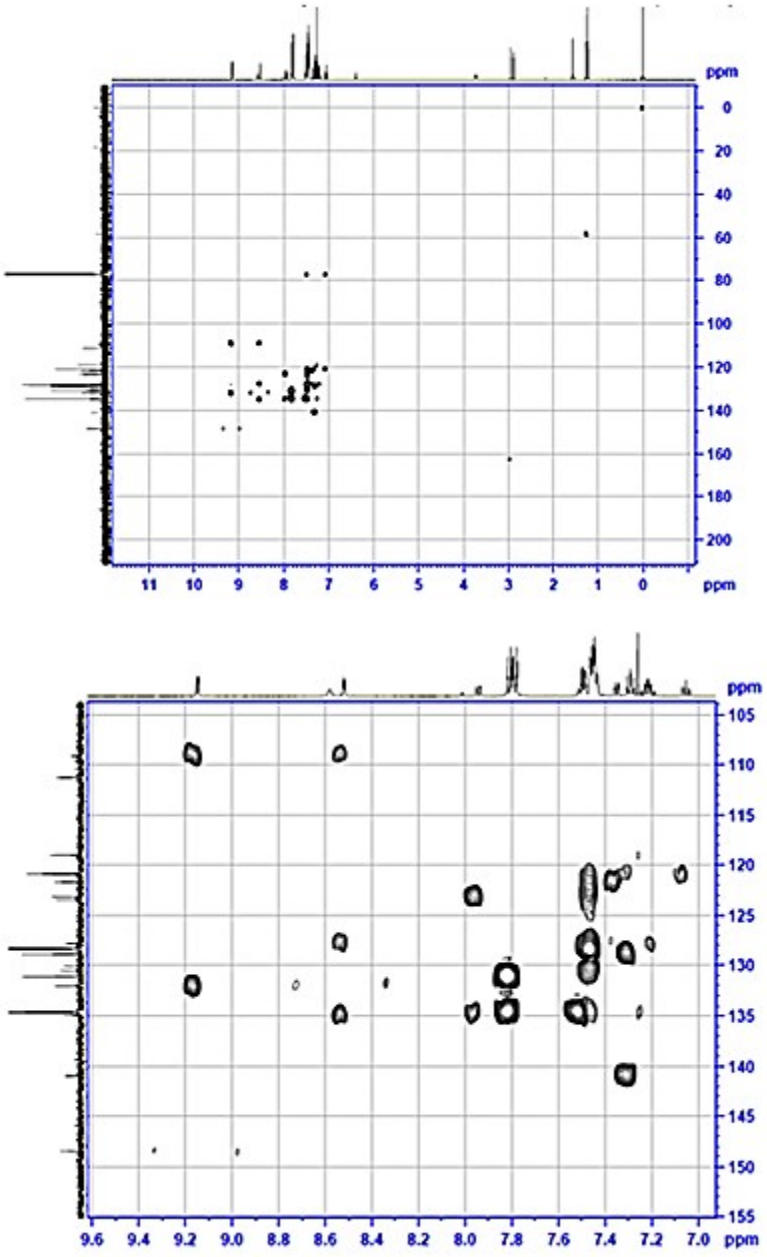

Figure S28. $^{1}H–^{13}C$ HMBC and expansion of $^{1}H–^{13}C$ HMBC spectrum of **5**.

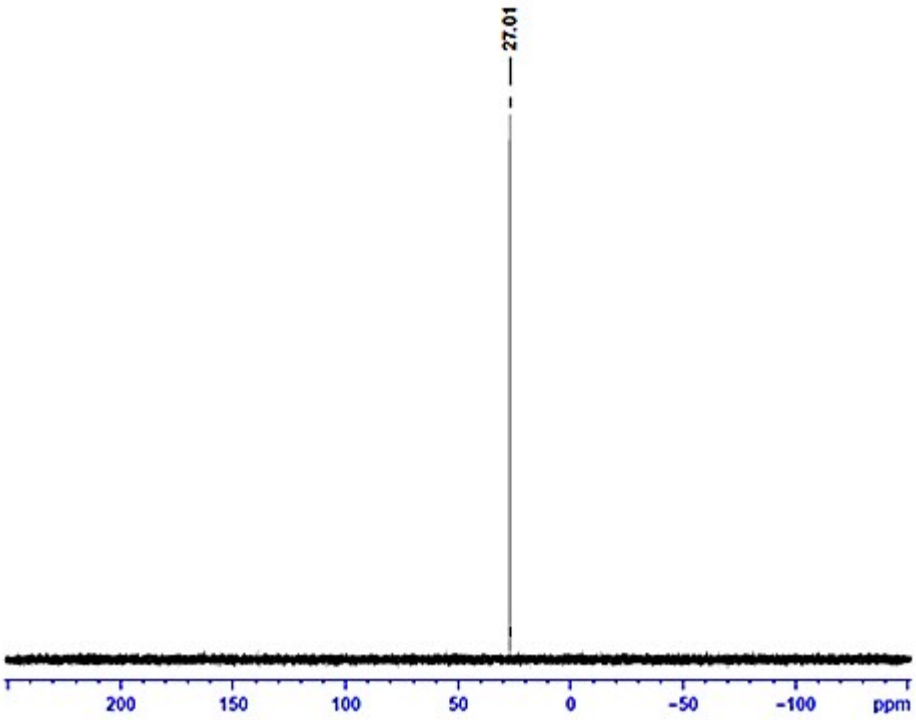

Figure S29. ^{31}P NMR spectrum of **1**.

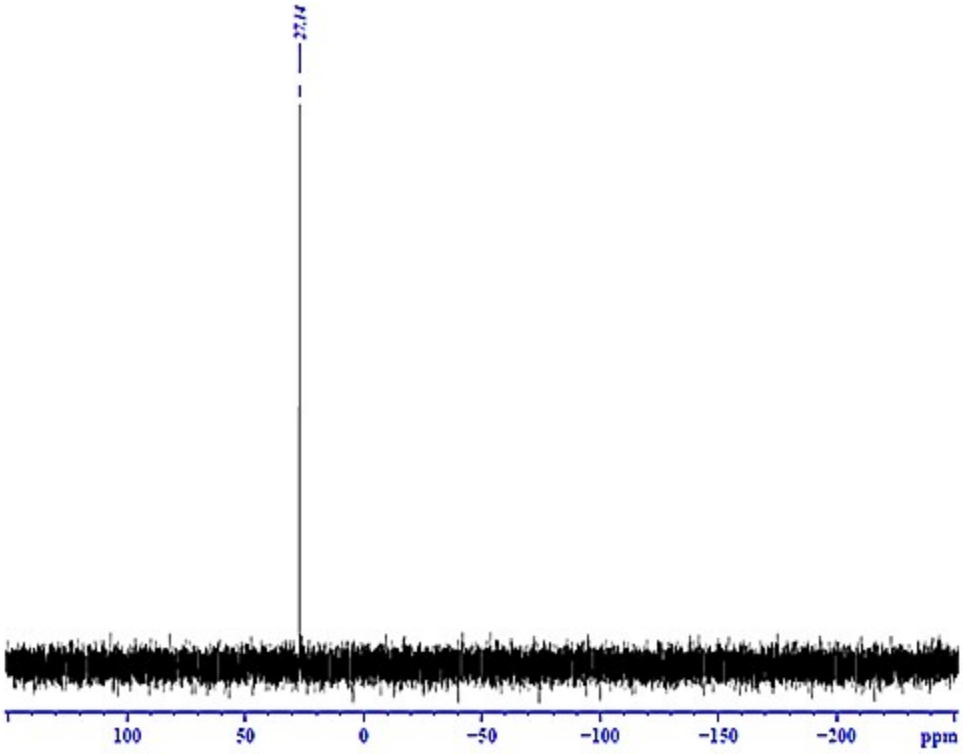

Figure S30. ^{31}P NMR spectrum of **2**.

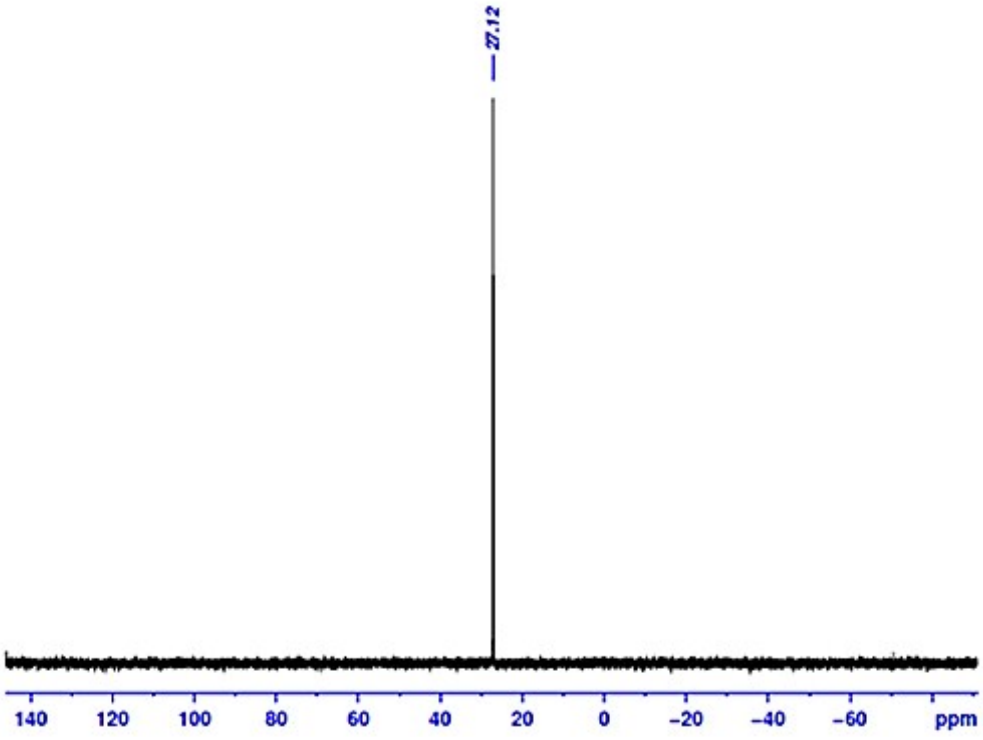

Figure S31. ^{31}P NMR spectrum of **3**.

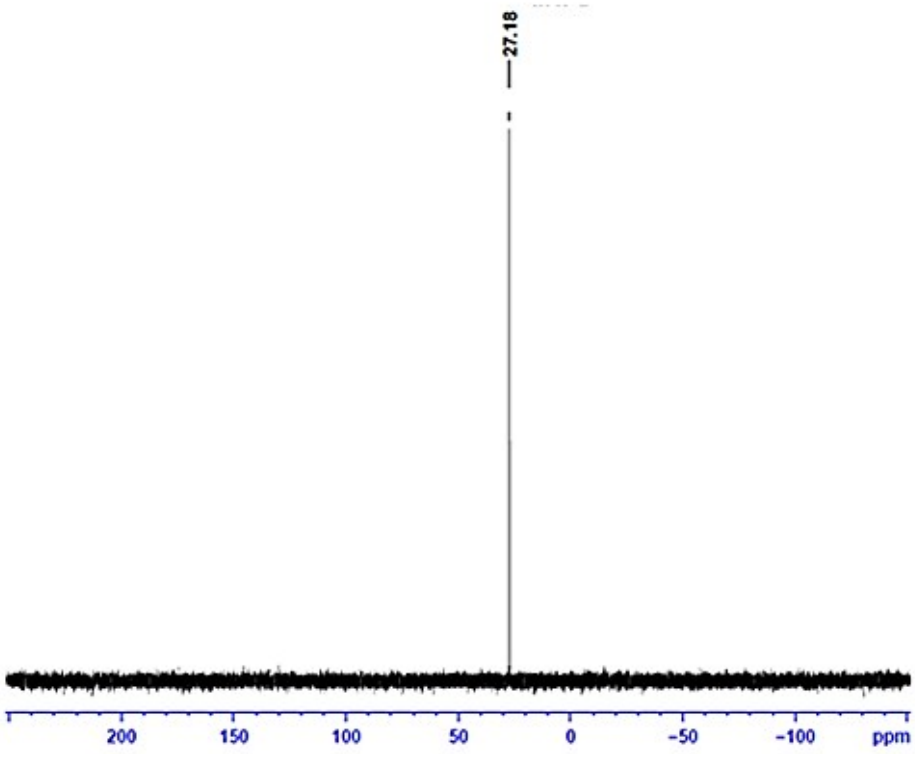

Figure S32. ^{31}P NMR spectrum of **4**.

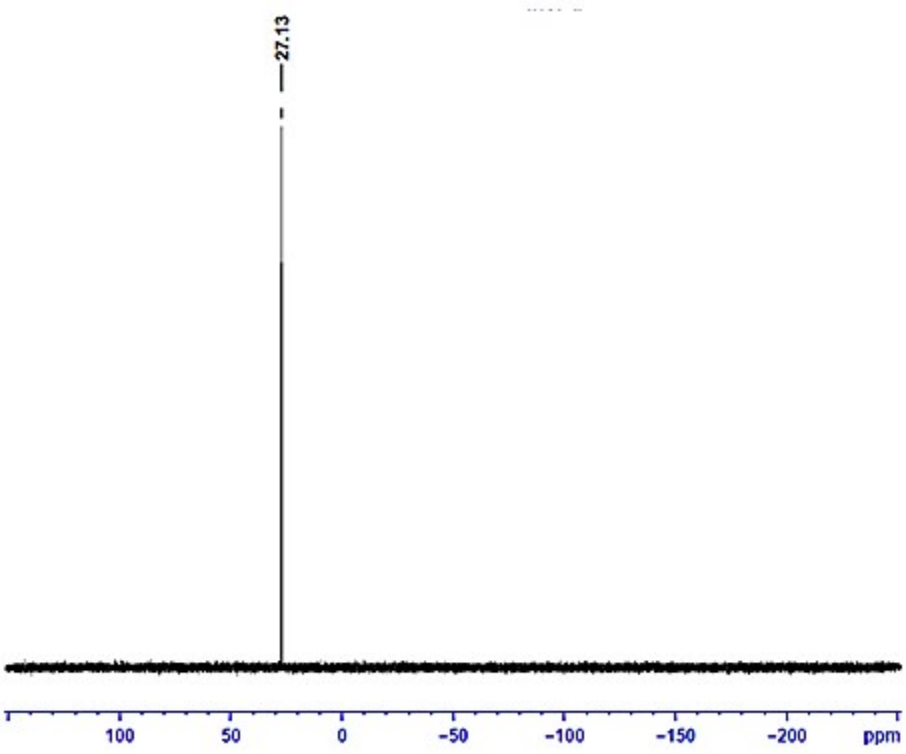

Figure S33. ^{31}P NMR spectrum of **5**.

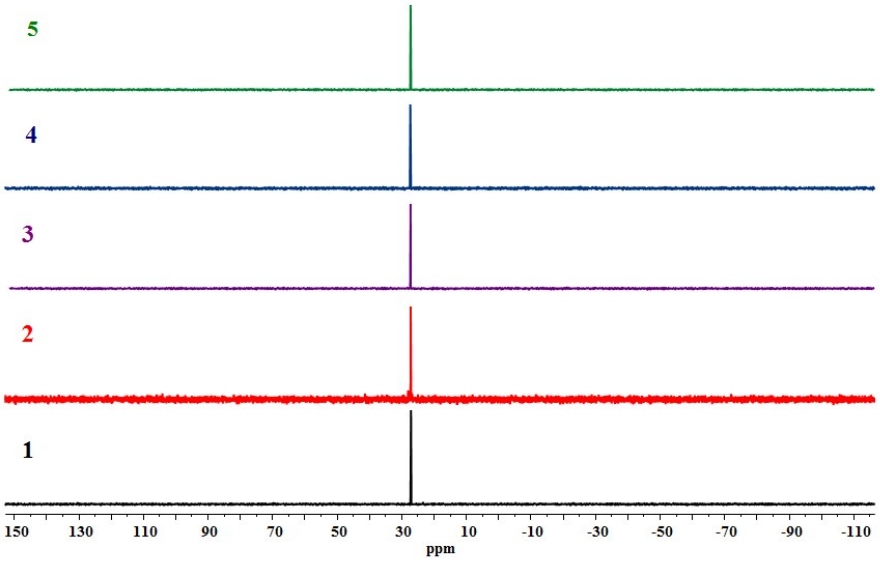

Figure S34. ^{31}P NMR spectra of the palladium(II) complexes (**1**-**5**).

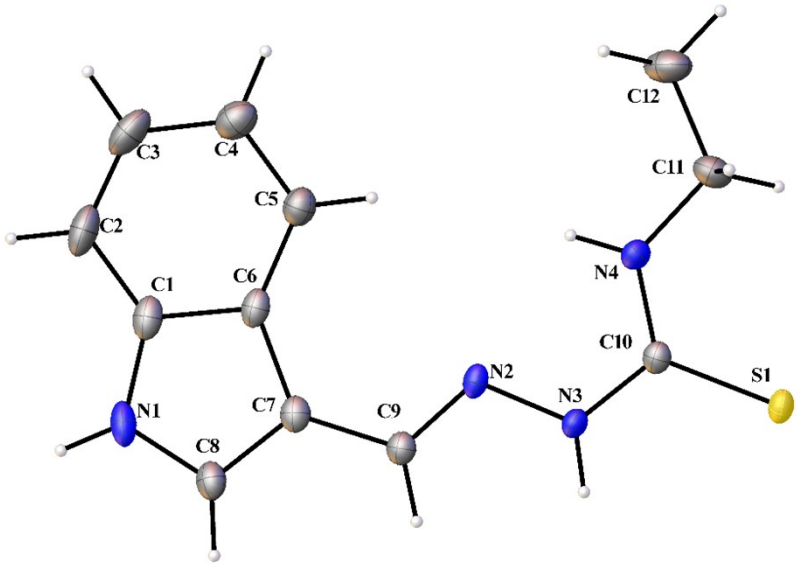

Figure S35. Thermal ellipsoid plot of HL3. Selected bond distances (Å) and angles (°): S(1)–C(10) 1.6995(15), N(2)–N(3) 1.3818(16), C(9)–N(2)–N(3) 115.67(12), C(10)–N(3)–N(2) 119.01(12), N(3)–C(10)–S(1) 120.37(11), N(4)–C(10)–S(1) 123.03(11), N(4)–C(10)–N(3) 116.57(13). Selected torsion angles (°): N(2)–N(3)–C(10)–S(1) −177.04(10), N(2)–N(3)–C(10)–N(4) 1.16(19), N(3)–N(2)–C(9)–C(7) −178.00(12), C(9)–N(2)–N(3)–C(10) 178.22(12), C(11)–N(4)–C(10)–S(1) −6.1(2).

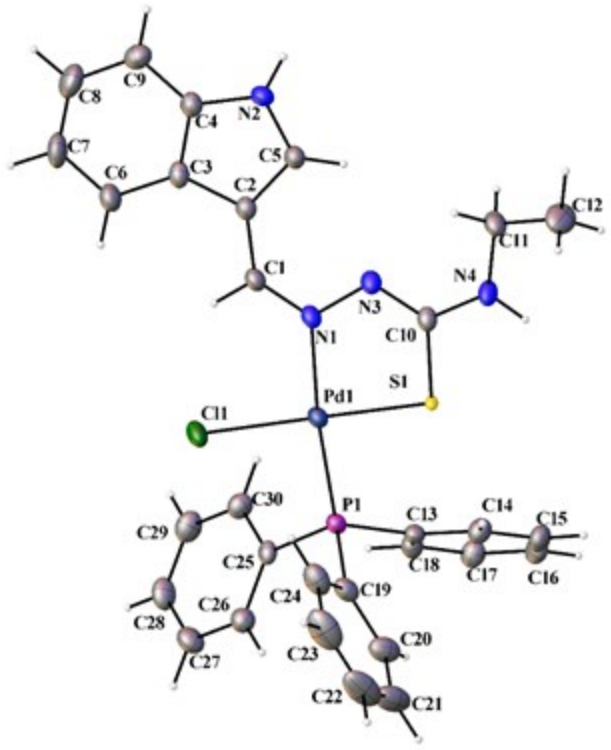

Figure S36. Thermal ellipsoid plot of **3**. Selected bond distances (Å) and angles (°): Pd(1)–Cl(1) 2.3363(12), Pd(1)–P(1) 2.2476(13), Pd(1)–N(1) 2.077(4), Pd(1)–S(1) 2.232(3), P(1)–Pd(1)–Cl(1) 87.85(5), N(1)–Pd(1)–Cl(1) 96.54(11), N(1)–Pd(1)–P(1) 175.07(12), N(1)–Pd(1)–S(1) 84.1(5), S(1)–Pd(1)–Cl(1) 176.6(7), S(1)–Pd(1)–P(1) 91.4(5), N(3)–N(1)–Pd(1) 120.1(2). Selected torsion angles (°): Pd(1)–N(1)–N(3)–C(10) −1.7(4), Pd(1)–S(1)–C(10)–N(3) −3.1(4), Pd(1)–S(1)–C(10)–N(4) 176.7(3).

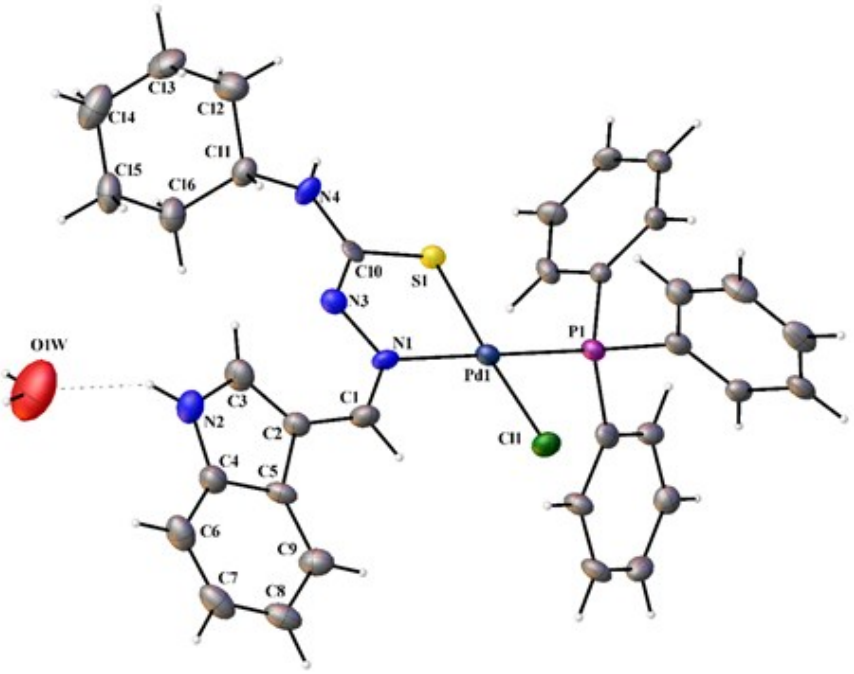

Figure S37. Thermal ellipsoid plot of **4** (some of the atoms are not labelled for clarity). Selected bond distances (Å) and angles (°): Pd(1)–Cl(1) 2.3453(14), Pd(1)–P(1) 2.2585(14), Pd(1)–N(1) 2.077(5), Pd(1)–S(1) 2.2476(15), P(1)–Pd(1)–Cl(1) 89.53(5), N(1)–Pd(1)–Cl(1) 93.93(13), N(1)–Pd(1)–P(1) 175.09(14), N(1)–Pd(1)–S(1) 83.31(13), S(1)–Pd(1)–Cl(1) 171.11(5), S(1)–Pd(1)–P(1) 93.78(5), N(3)–N(1)–Pd(1) 120.3(3). Selected torsion angles (°): Pd(1)–N(1)–N(3)–C(10) 7.8(6), Pd(1)–S(1)–C(10)–N(3) −10.9(5), Pd(1)–S(1)–C(10)–N(4) 172.2(4).

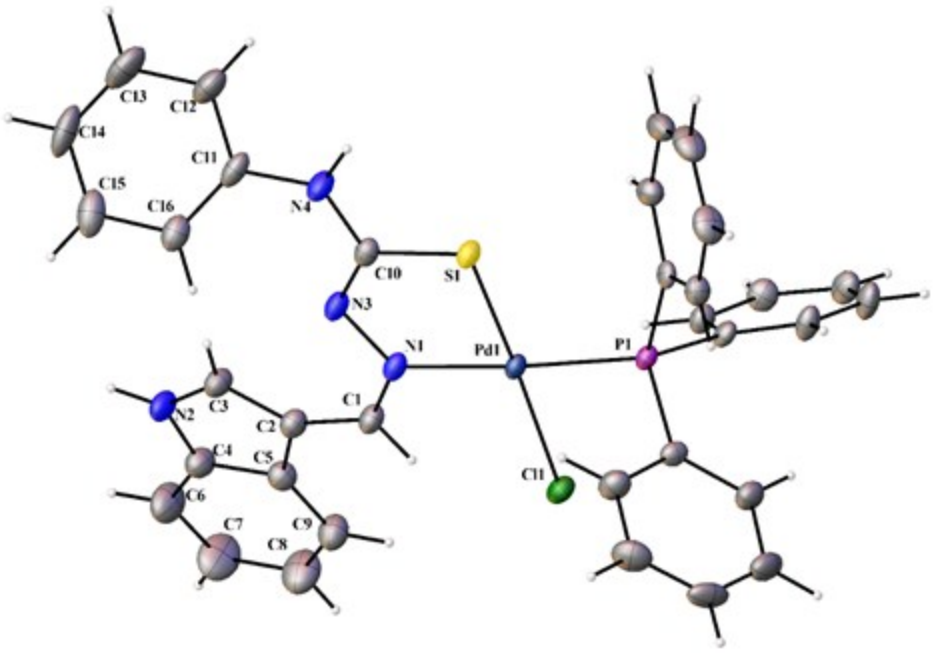

Figure S38. Thermal ellipsoid plot of **5** (some of the atoms are not labelled for clarity). Selected bond distances (Å) and angles (°): Pd(1)–Cl(1) 2.3639(8), Pd(1)–P(1) 2.2582(6), Pd(1)–N(1) 2.0770(19), Pd(1)–S(1) 2.2331(8), P(1)–Pd(1)–Cl(1) 86.92(2), N(1)–Pd(1)–Cl(1) 96.16(6), N(1)–Pd(1)–P(1) 176.39(6), N(1)–Pd(1)–S(1) 82.68(5), S(1)–Pd(1)–Cl(1) 177.06(3), S(1)–Pd(1)–P(1) 94.33(2), N(3)–N(1)–Pd(1) 121.52(14). Selected torsion angles (°):Pd(1)–N(1)–N(3)–C(10) –0.2(3), Pd(1)–S(1)–C(10)–N(3) 1.7(2), Pd(1)–S(1)–C(10)–N(4) –176.94(15).

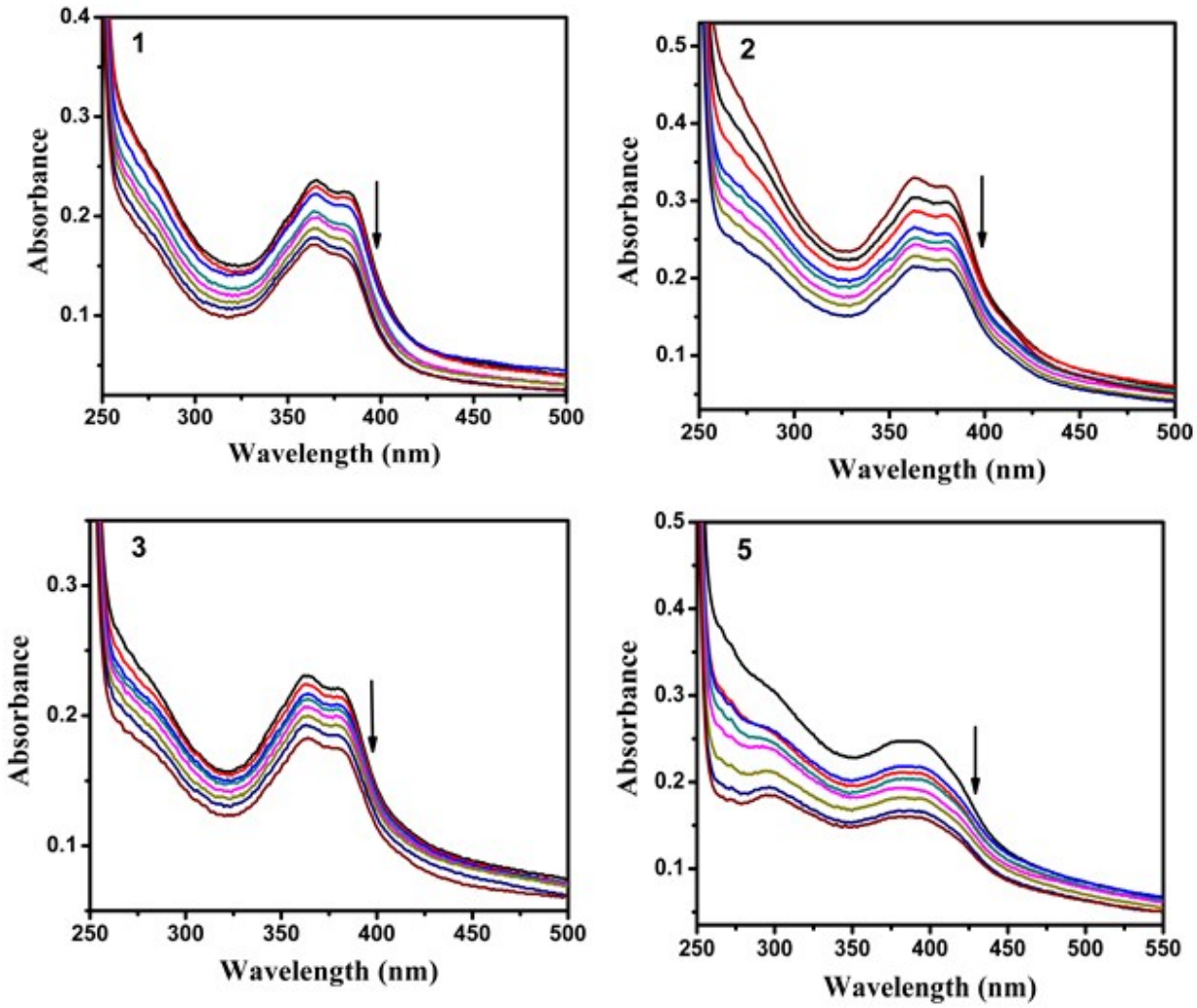

Figure S39. Absorption spectra of complexes (**1-3** and **5**) in Tris-HCl buffer upon addition of CT DNA. [Complex] = 2.0 × 10^{-5} M, [DNA] = 0-35 μM. The arrow shows that the absorption intensities decrease upon increasing DNA concentration.

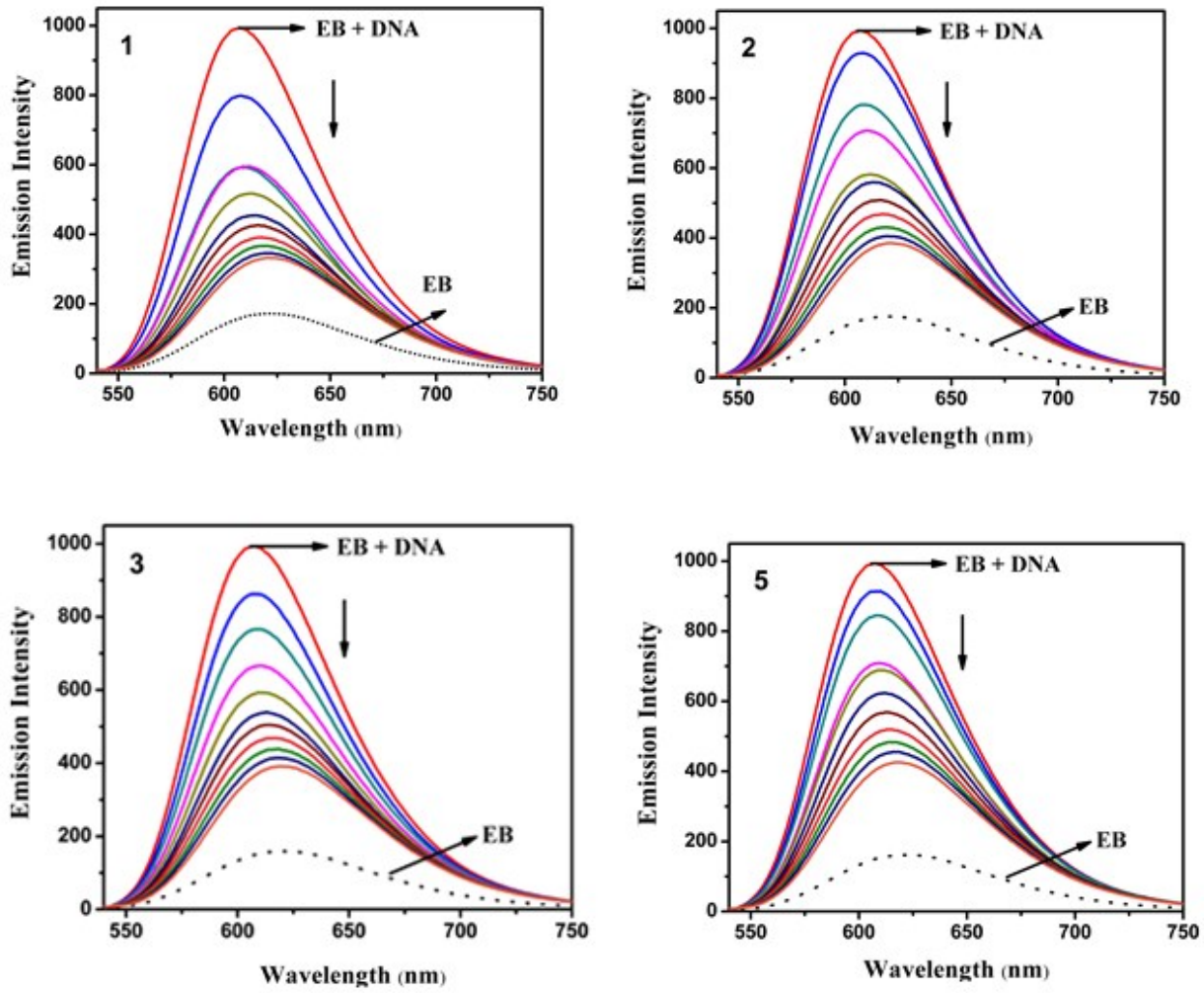

Figure S40. Fluorescence quenching curves of EB bound to DNA in the presence of **1-3** and **5**. [DNA] = 5 μM, [EB] = 5 μM and [complex] = 0-50 μM.

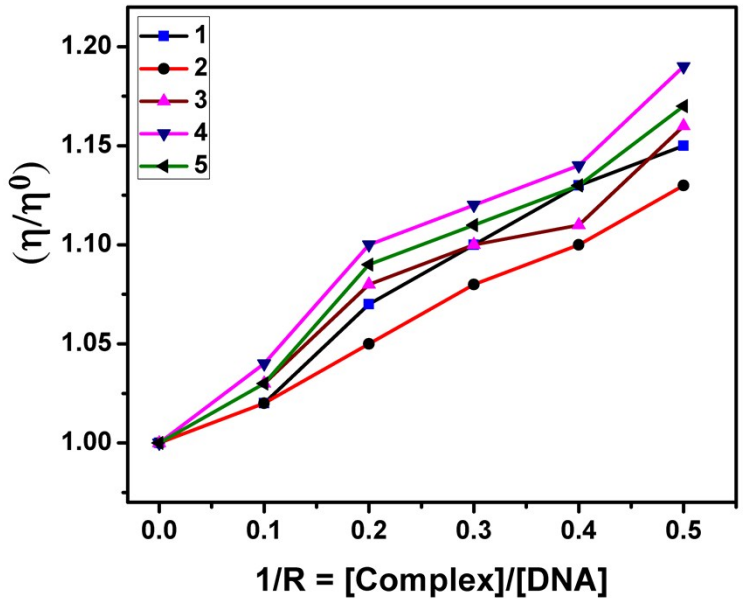

Figure S41. Effect of the complexes (**1**-**5**) on the viscosity of CT DNA.

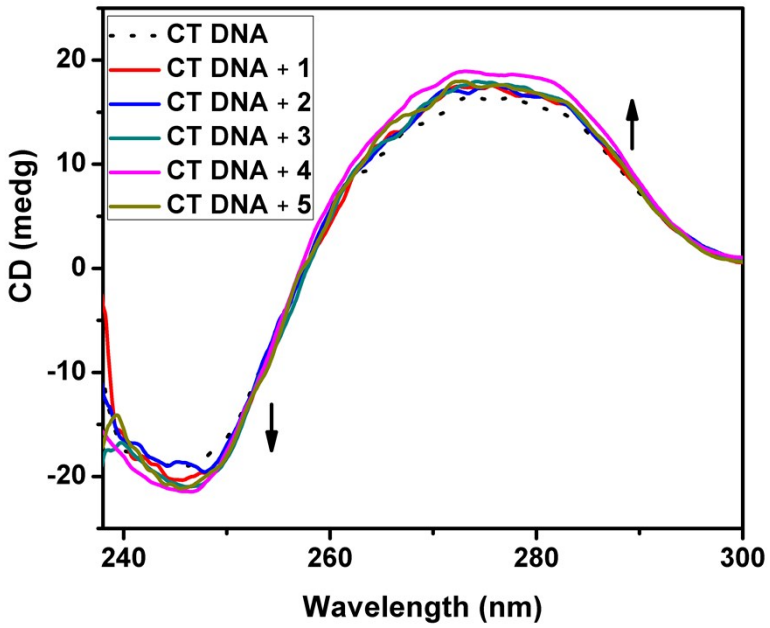

Figure S42. CD spectra of CT DNA in the absence and presence of the complexes in Tris-HCl buffer (pH 7.2) at room temperature. [Complex] = 5 μM, [DNA] = 20 μM.

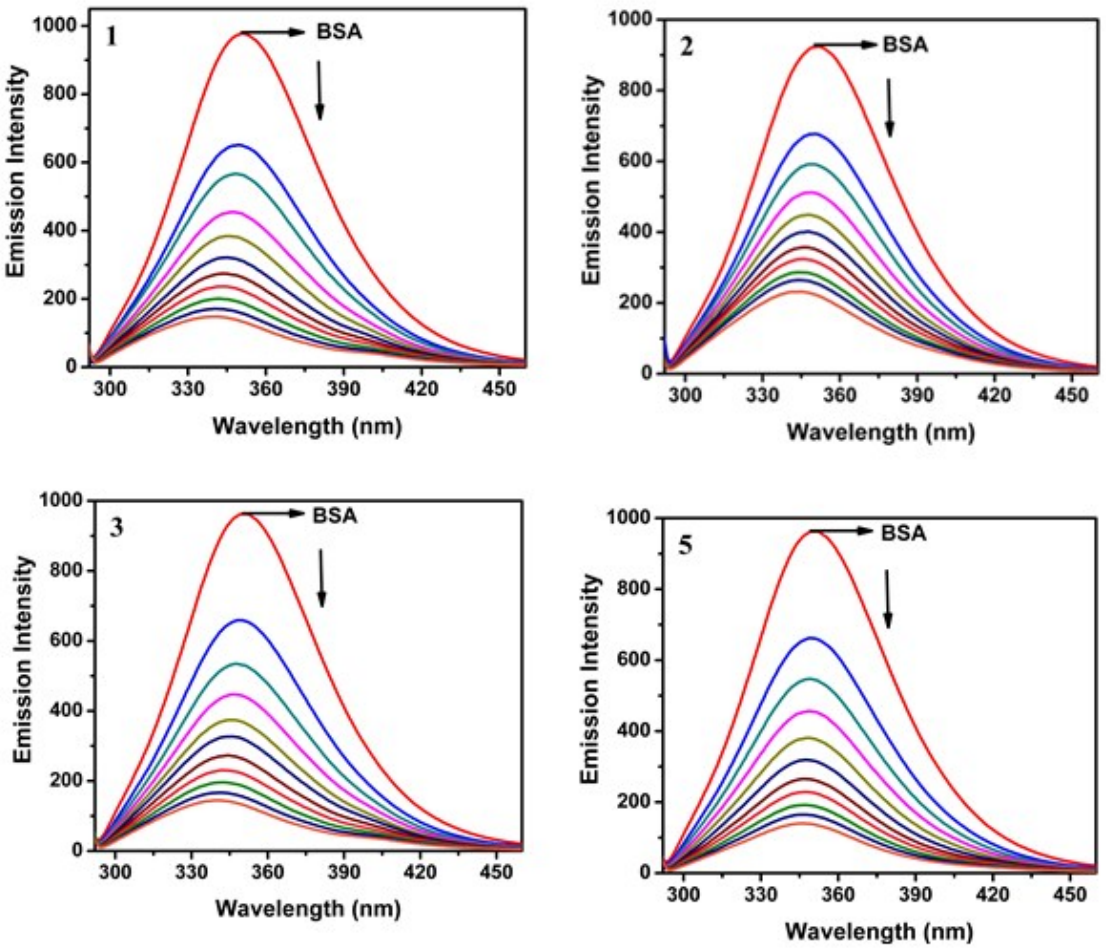

Figure S43. Fluorescence quenching curves of BSA in the absence and presence of **1-3** and **5**. [BSA] = 1 μM and [complex] = 0-20 μM.

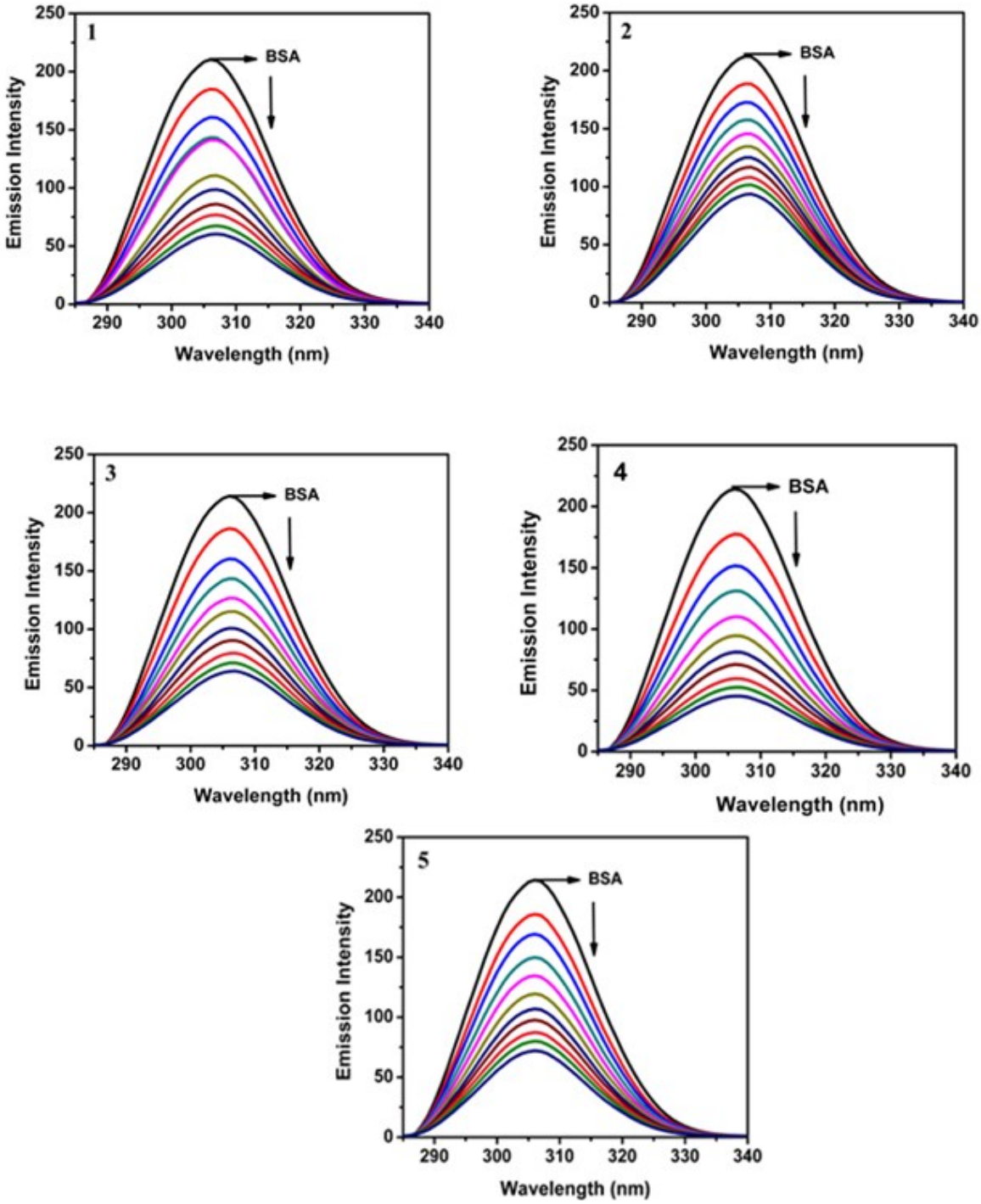

Figure S44. Synchronous spectra of BSA (1 μM) as a function of concentration of **1**, **2**, **3**, **4** and **5** (0-20 μM), when $\Delta\lambda$ = 15 nm.

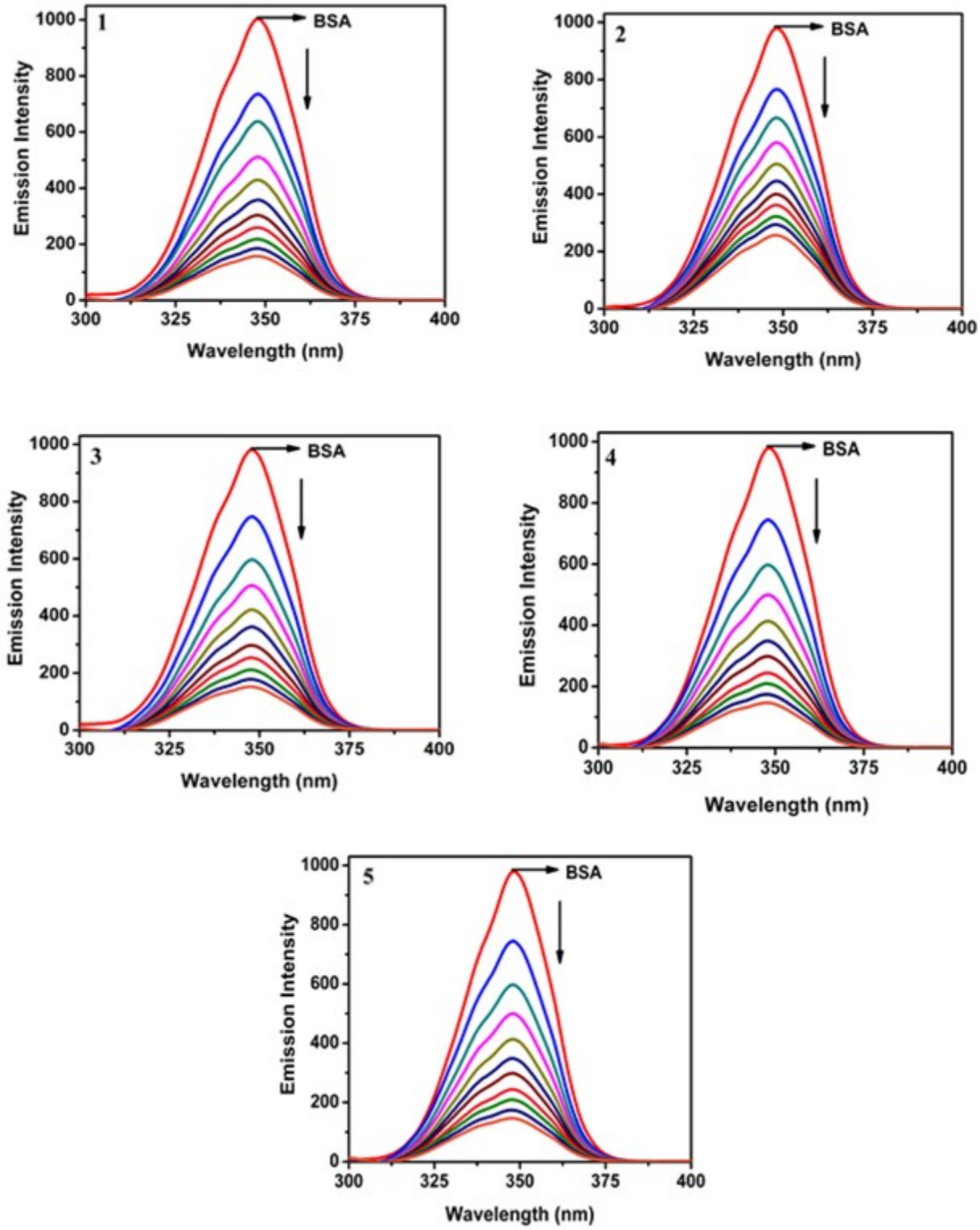

Figure S45. Synchronous spectra of BSA (1 μM) as a function of concentration of **1**, **2**, **3**, **4** and **5** (0-20 μM), when $\Delta\lambda$ = 60 nm.

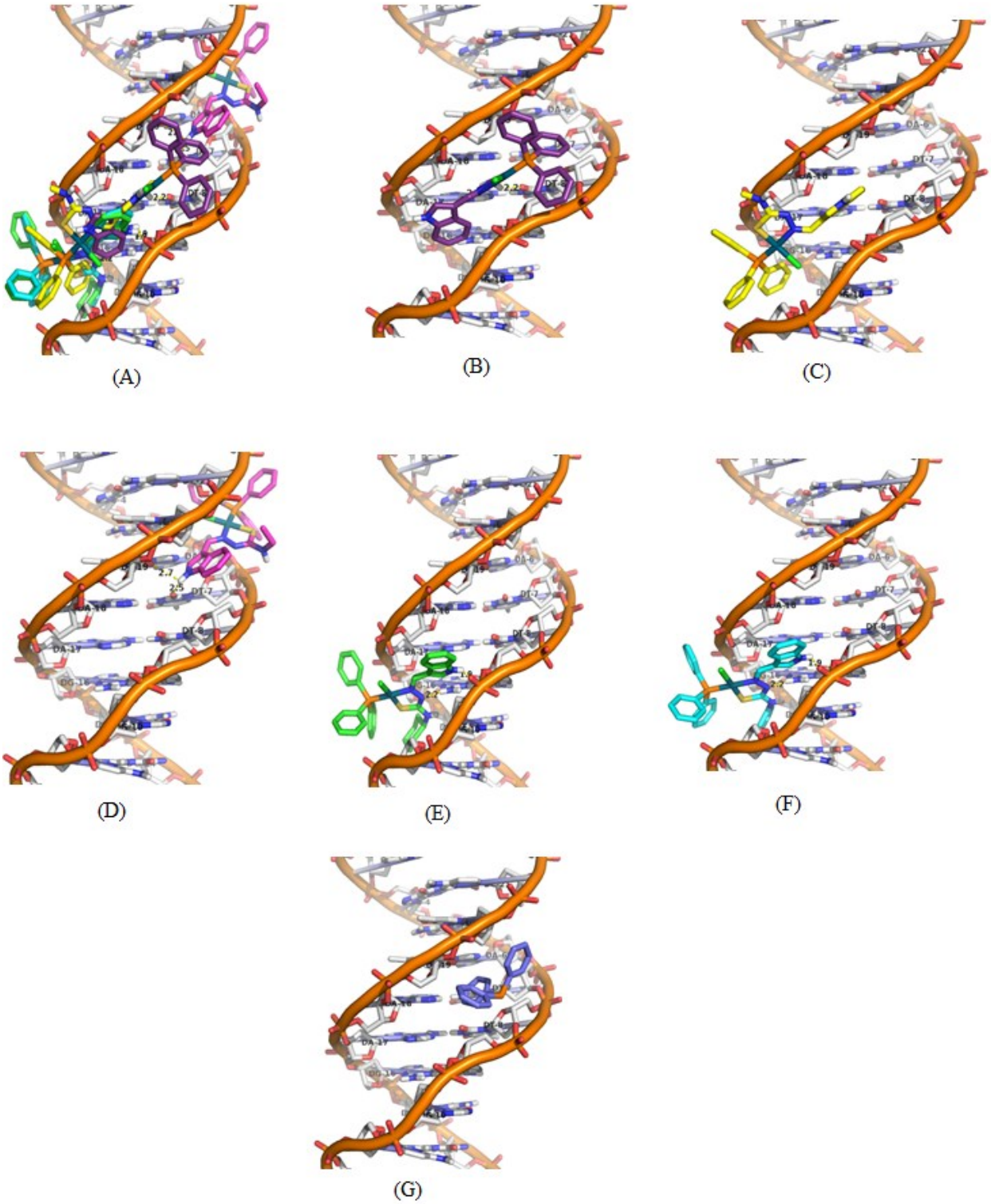

Figure S46. Docking of the palladium(II) complexes with B-DNA. (PDB: 1BNA); (A) Docking pose of **1-5**. (B) Docking pose of **1**; (C) Docking pose of **2**; (D) Docking pose of **3**; (E) Docking pose of **4**; (F) Docking pose of **5** and (G) Docking pose of PPh_3.

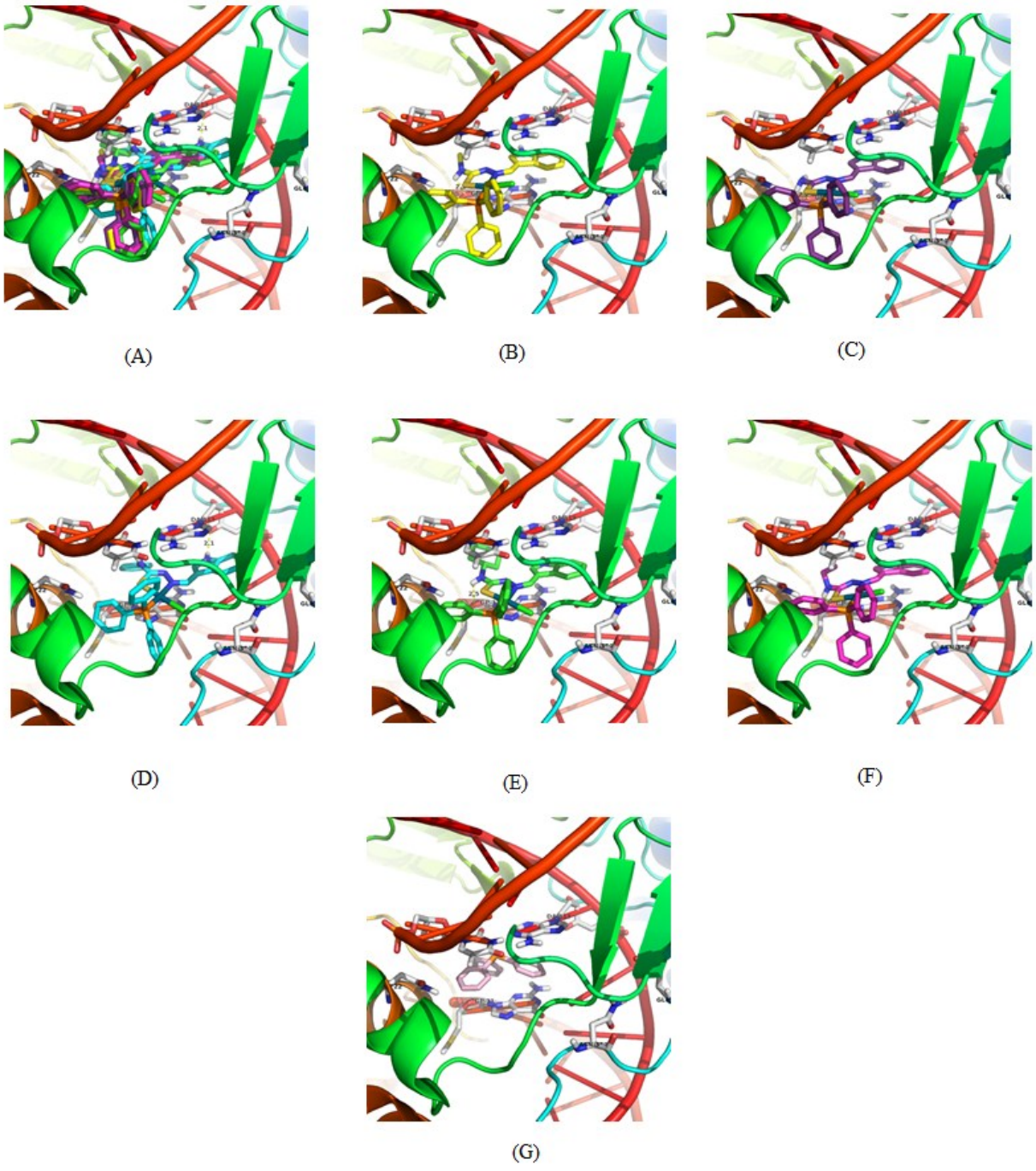

Figure S47. Docking of the compounds with DNA-Topoisomerase I (PDB: 1SC7); (A) Docking pose of **1**-**5**. (B) Docking pose of **1**; (C) Docking pose of **2**; (D) Docking pose of **3**; (E) Docking pose of **4**; (F) Docking pose of **5** and (G) Docking pose of PPh_3.

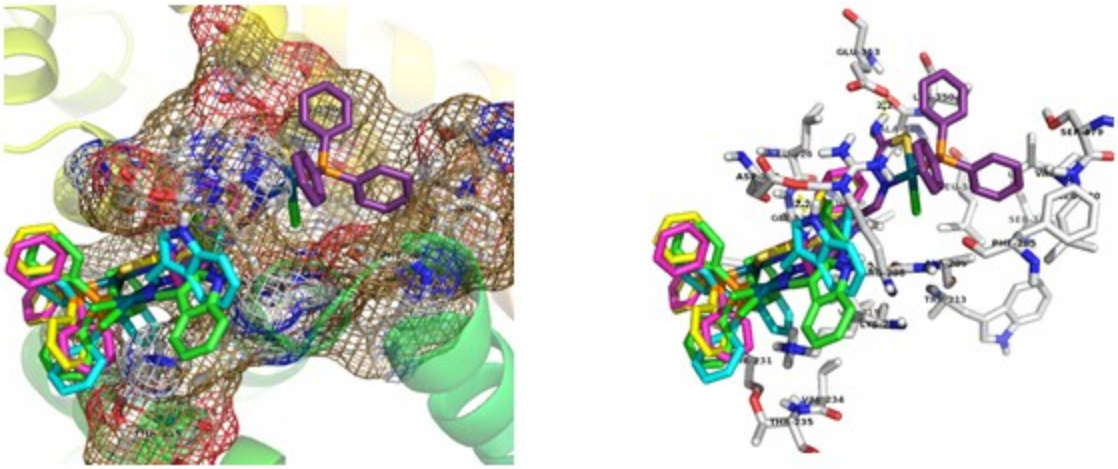

(A)

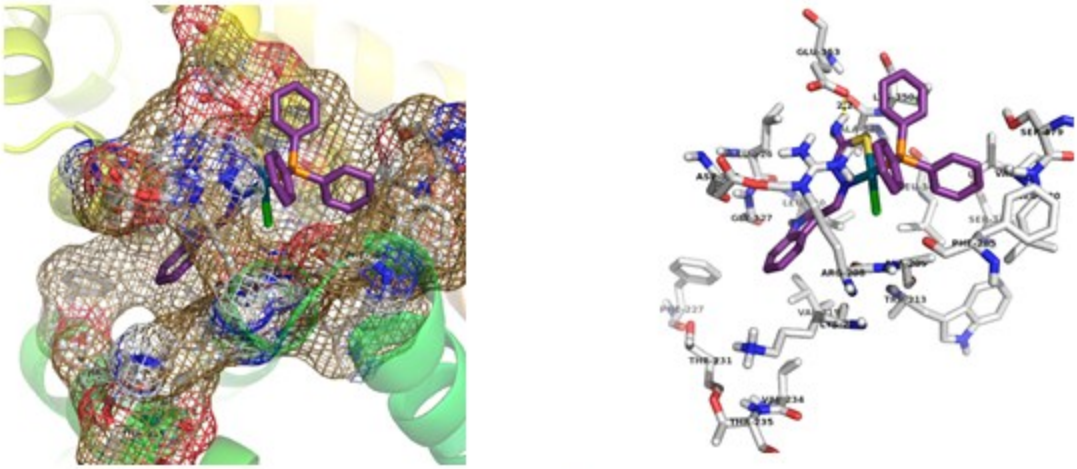

(B)

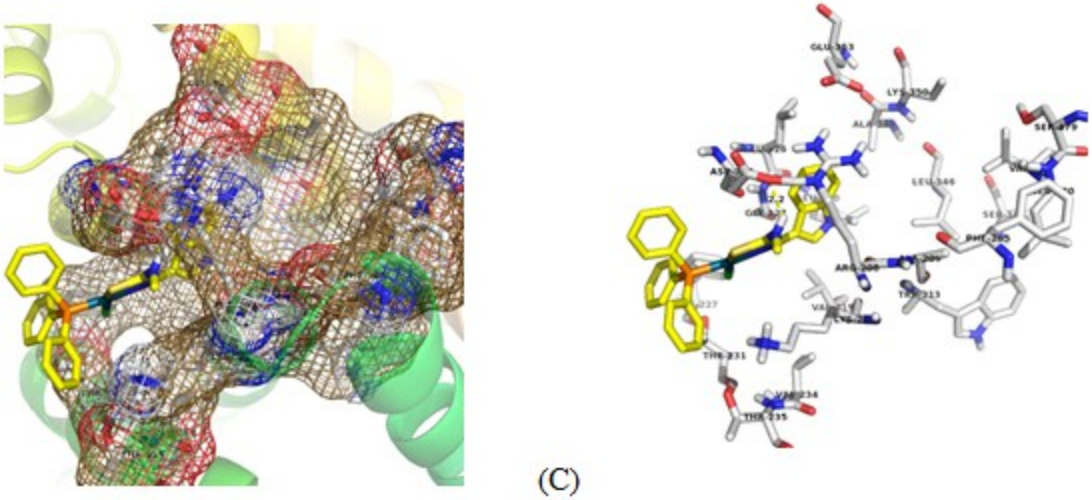

(C)

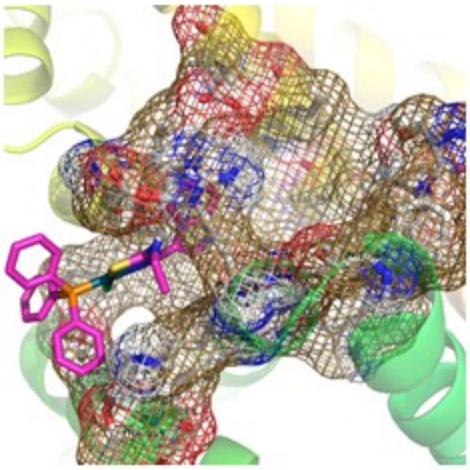

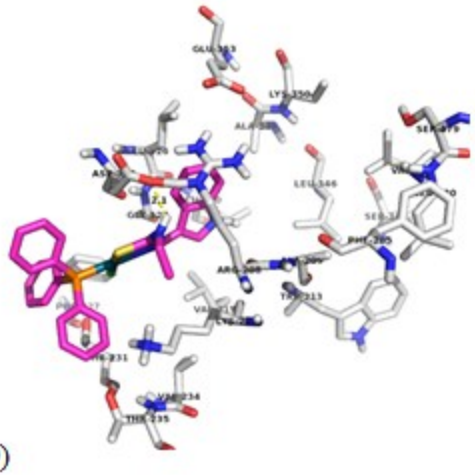

(D)

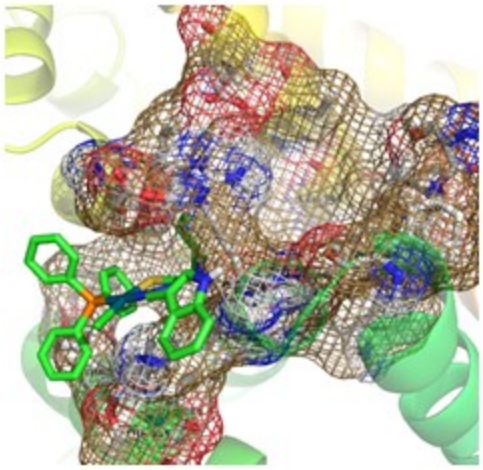

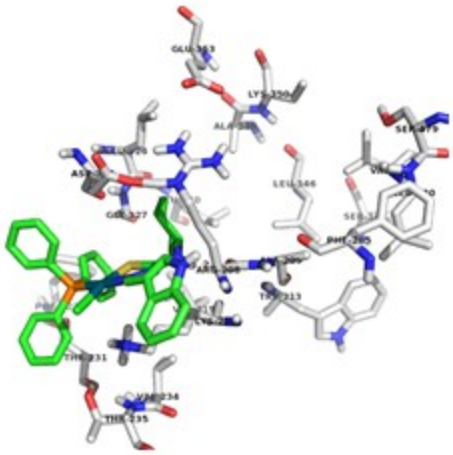

(E)

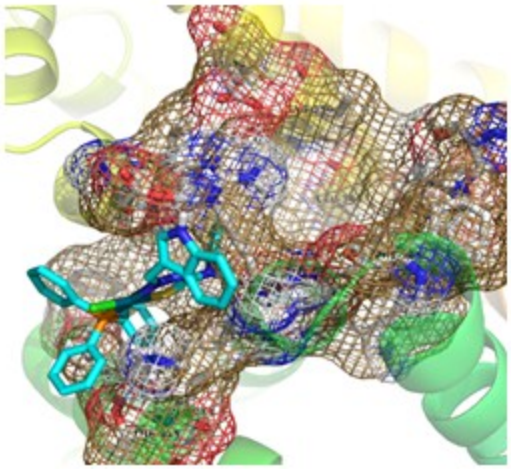

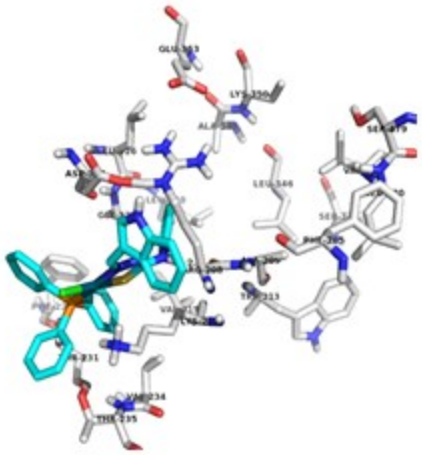

(F)

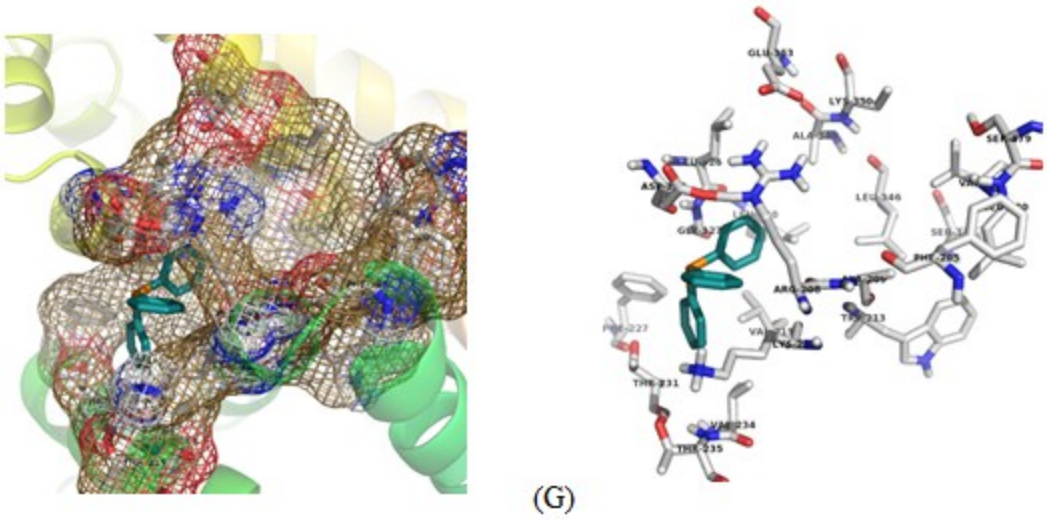

Figure S48. Docking of the compounds with BSA (PDB: 3V03; (A) Docking pose of **1**-**5**. (B) Docking pose of **1**; (C) Docking pose of **2**; (D) Docking pose of **3**; (E) Docking pose of **4**; (F) Docking pose of **5** and (G) Docking pose of PPh_3.

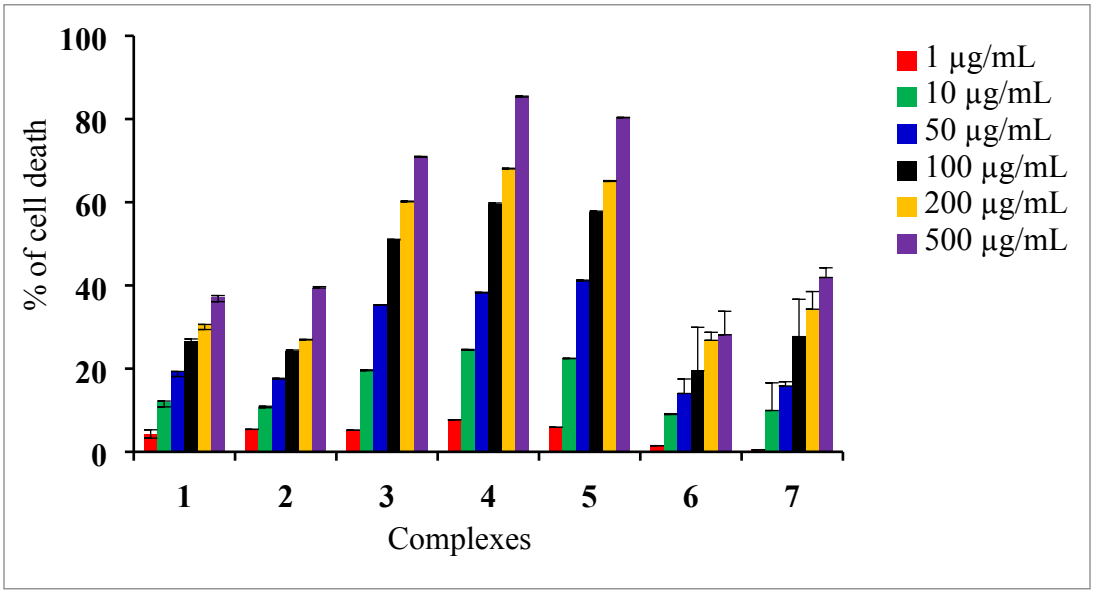

Figure S49. Comparison of anticancer activity of complexes (**1**-**7**) against MCF7 cancer cells. Data are mean ± SD of three independent experiments with each experiment conducted in triplicate. Positive control: Cisplatin 12.0 (IC_{50}).

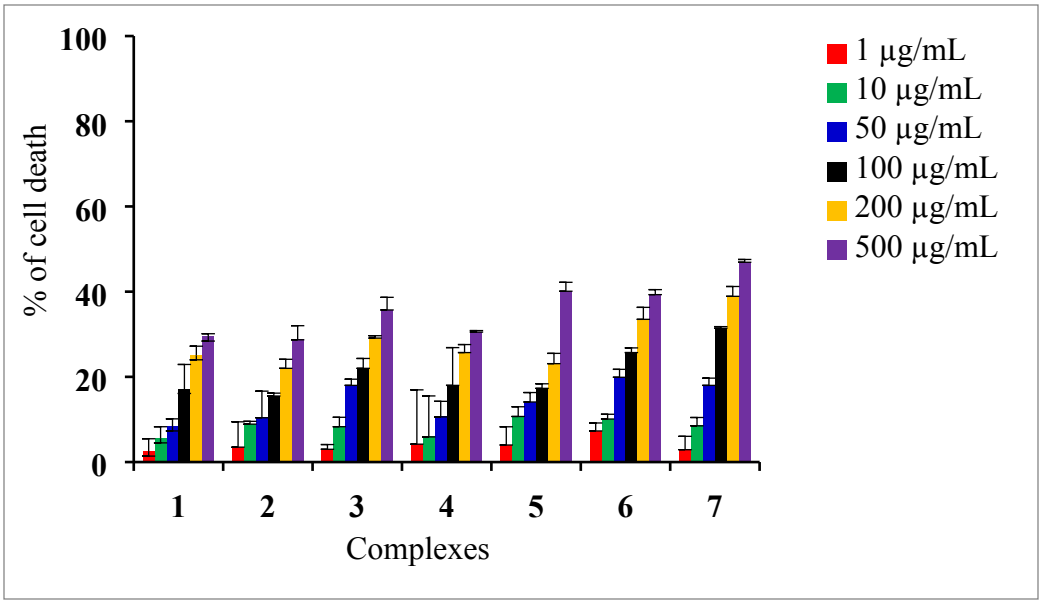

Figure S50. Comparison of anticancer activity of complexes (**1-7**) against L929 normal cells. Data are mean ± SD of three independent experiments with each experiment conducted in triplicate. Positive control: Cisplatin 6.0 (IC_{50}).

Table S1. Experimental data for crystallographic analysis of L3, **2** and **3**

	HL3	**2**	**3**
Empirical formula	$C_{12}H_{14}N_4S$	$C_{32}H_{33}ClN_5OPPdS$	$C_{33}H_{35}ClN_5OPPdS$
Formula weight	246.33	708.51	722.54
Temperature (K)	110.15	150.15	150.15
Wavelength (Å)	0.71073	0.71073	0.71073
Crystal system	Monoclinic	Monoclinic	Monoclinic
Space group	$P2_1/c$	$P2_1/c$	$P2_1/c$
Unit cell dimensions			
a (Å)	15.073(5)	17.995(4)	32.724(9)
b (Å)	4.9158(16)	9.0166(19)	8.830(2)
c (Å)	16.419(5)	20.915(4)	35.834(10)

α (°)	90	90	90
β (°)	99.242(4)	110.053(2)	108.159(3)
γ (°)	90	90	90
Volume (Å^3)	1200.7(7)	3187.9(12)	9838(5)
Z	4	4	12
Density (calculated) Mg/m^3	1.363	1.476	1.463
Absorption coefficient (mm^{-1})	0.252	0.815	0.794
F(000)	520	1448	4440
Crystal size (mm^3)	0.57 × 0.31 × 0.22	0.35 × 0.24 × 0.18	0.5 × 0.24 × 0.14
Theta range for data collection (°)	2.514 to 27.360	2.009 to 27.612	0.655 to 27.560
Index ranges	–19<=h<=19, –6<=k<=6, –20<=l<=21	–23<=h<=23, –11<=k<=11, –26<=l<=26	–42<=h<=42, –11<=k<=11, –46<=l<=46
Reflections collected	12650	34644	111386
Independent reflections [R(int)]	2698 0.0387	7342 0.0322	22425 0.0733
Completeness to theta = 25.242°	99.8 %	99.9 %	99.9 %
Absorption correction	Semi-empirical from equivalents	Semi-empirical from equivalents	Semi-empirical from equivalents
Max. and min. transmission	0.7456 and 0.6390	0.7456 and 0.6382	0.7362 and 0.5761
Refinement method	Full-matrix least-squares on F^2	Full-matrix least-squares on F^2	Full-matrix least-squares on F^2

Data / restraints / parameters	2698 / 0 / 155	7342 / 0 / 382	22425 / 34 / 1165
Goodness-of-fit on F^2	1.026	1.024	1.088
Final R indices [I>2sigma(*I*)]	R1 = 0.0348, wR2 = 0.0816	R1 = 0.0223, wR2 = 0.0556	R1 = 0.0539, wR2 = 0.1084
R indices (all data)	R1 = 0.0410, wR2 = 0.0847	R1 = 0.0269, wR2 = 0.0583	R1 = 0.0713, wR2 = 0.1163
Largest diff. peak and hole (e.Å^{-3})	0.289 and –0.273	0.413 and –0.449	3.163 and –1.373

Table S2. Experimental data for crystallographic analysis of **4**, **5** and **6**

	4	**5**	**6**
Empirical formula	$C_{34}H_{34\cdot50}ClN_4O_{0.25}PPdS$	$C_{34}H_{28}ClN_4PPdS$	$C_{28}H_{36}N_{10}O_2PdS_2$
Formula weight	708.03	697.48	715.19
Temperature (K)	110.15	110.15	99.97
Wavelength (Å)	1.54178	0.71073	0.71073
Crystal system	Monoclinic	Monoclinic	Triclinic
Space group	*P2/n*	*Pc*	*P*$\bar{1}$
Unit cell dimensions			
a (Å)	9.5377(5)	10.0748(19)	8.4859(5)
b (Å)	9.5497(5)	11.326(2)	10.467(6)
c (Å)	35.8336(14)	15.049(3)	10.4763(6)
α (°)	90	90	62.2180(10)
β (°)	94.015(3)	96.909(2)	71.7410(10)

γ(°)	90	90	78.4310(10)
Volume (Å^3)	3255.8(3)	1704.7(6)	780.19(8)
Z	4	2	1
Density (calculated) Mg/m^3	1.444	1.359	1.522
Absorption coefficient (mm^{-1})	6.651	0.759	0.773
F(000)	1450	708	368
Crystal size (mm^3)	0.04 × 0.04 × 0.03	0.32 × 0.29 × 0.07	0.51 × 0.17 × 0.05
Theta range for data collection (°)	2.472 to 60.814	1.798 to 27.344	2.383 to 27.595
Index ranges	–10<=h<=9, –10<=k<=10, –40<=l<=40	–12<=h<=12, –14<=k<=14, –19<=l<=19	–11<=h<=11, –13<=k<=13, –13<=l<=13
Reflections collected	22035	18810	16232
Independent reflections [R(int)]	4642 0.0794	7602 0.0144	3596 0.0181
Completeness to theta = 25.242°	78.6 %	100.0 %	99.7 %
Absorption correction	Semi-empirical from equivalents	Semi-empirical from equivalents	Semi-empirical from equivalents
Max. and min. transmission	0.7519 and 0.6041	0.7456 and 0.5872	0.7456 and 0.0181
Refinement method	Full-matrix least-squares on F^2	Full-matrix least-squares on F^2	Full-matrix least-squares on F^2
Data / restraints / parameters	4642 / 0 / 388	7602 / 2 / 379	3596 / 0 / 199
Goodness-of-fit on	1.054	1.043	1.097

F^2			
Final R indices [I>2sigma(*I*)]	R1 = 0.0488, wR2 = 0.1166	R1 = 0.0151, wR2 = 0.0396	R1 = 0.0179, wR2 = 0.0461
R indices (all data)	R1 = 0.0638, wR2 = 0.1221	R1 = 0.0155, wR2 = 0.0398	R1 = 0.0186, wR2 = 0.0465
Largest diff. peak and hole (e.Å^{-3})	0.740 and –0.912	0.260 and –0.235	0.334 and –0.699

Table S3. ^{31}P NMR spectral data of the Pd(II) complexes

Complex	Chemical shift in ppm
[PdCl(L1)(PPh_3)] (**1**)	27.01 (s)
[PdCl(L2)(PPh_3)] (**2**)	27.14 (s)
[PdCl(L3)(PPh_3)] (**3**)	27.12 (s)
[PdCl(L4)(PPh_3)] (**4**)	27.18 (s)
[PdCl(L5)(PPh_3)] (**5**)	27.13 (s)

Table S4. Hydrogen bonding in complexes **2** and **4**

Complex	d(D-H)	d(H...A)	d(D...A)	<(DHA)
2				
N(3)–H(3)...O(1S)	0.88	1.98	2.7958(19)	154.5
4				
N(2)–H(2)...O(1W)	0.88	2.06	2.79(3)	139.9

Symmetry transformations used to generate equivalent atoms:

#1 -x+2,y+1/2,-z+1/2 (**2**), #1 -x+1, -y, -z+2 (**4**)

Table S5. *In vitro* cytotoxic studies of the complexes against HepG-2, A549, MCF7 cancer and L929 normal cell lines

	IC_{50} (μM)			
Complex	HepG-2	A549	MCF7	L929
1	93.5	111.5	> 500	> 800
2	110.4	> 200	> 500	> 800
3	74.5	128.6	139.4	> 800
4	22.8	94.1	111.8	> 800
5	67.1	91.5	116.1	> 700
6	> 100	> 100	> 100	> 880
7	96.3	80.4	> 100	552.9
Cisplatin	21.5	18.0	23.7	6

Elemental analysis for compounds

CHNS ANALYSIS RESULT *CAI-NIT Warangal*

Analytic Functional Testing
ICP-OES 720 series
VarioEL III CHNS
Serial Number 931
Ref. No: CAI/CH/160920A

Sample No	Sample Name	N%	C%	S%	H%	Sample Weight, mg	
1	L1	25.26	55.27	14.80	4.73	4.94	
2	L2	24.00	56.94	13.91	5.32	5.29	
3	L3	22.89	58.39	13.11	5.82	5.31	Ligand - L3
4	L4	18.86	64.37	10.90	6.43	5.01	
5	L5	19.37	65.41	10.94	4.65	5.27	

CHNS ANALYSIS RESULT *CAI-NIT Warangal*

Analytic Functional Testing
ICP-OES 720 series
VarioEL III CHNS
Serial Number 1032
Ref. No: CAI/CH/171223A

Sample No	Sample Name	N%	C%	S%	H%	Sample Weight, mg	
1	1	9.16	54.03	5.05	3.81	5.71	Complex - 1
2	2	8.90	54.75	5.11	4.04	5.10	Complex - 2
3	3	8.55	55.59	5.03	4.43	5.18	Complex - 3
4	4	8.09	57.97	4.50	4.81	6.06	Complex - 4
5	5	8.10	58.62	4.67	4.00	4.94	Complex - 5
6	6	20.86	44.39	11.71	3.50	4.89	
7	7	19.84	46.36	11.14	3.99	5.85	Complex - 6
8	8	18.94	48.16	10.57	4.56	6.31	
9	9	15.74	54.61	9.21	5.39	6.37	Complex - 7
10	10	16.35	55.31	9.37	3.96	5.35	

References

1 (a) S. Ramakrishnan and M. Palaniandavar, *Dalton Trans*., 2008, **29**, 3866-3878. (b) K. Jeyalakshmi, J. Haribabu, N. S. P. Bhuvanesh and R. Karvembu, *Dalton Trans.,* 2016, **45**, 12518-12531.

2 N. Selvakumaran, N. S. P. Bhuvanesh and R. Karvembu, *Dalton Trans.*, 2014, **43**, 16395-16410.

3 (a) V. I. Ivanov, L. E. Minchenkova, A. K. Schyolkina, A. I. Polytayer, *Biopolymers*, 1973, **12**, 89-110. (b) H. Pezzano and F. Podo, *Chem. Rev*., 1980, **80**, 365-401. (c) B. Saha, Md. M. Islam, S. Paul, S. Samanta, S. Ray, C. R. Santra, S. R. Choudhury, B. Dey, A. Das, S. Ghosh, S. Mukhopadhyay, G. S. Kumar and P. Karmakar, *J. Phys. Chem*. *B*, 2010, **114**, 5851-5861. (d) S. Mahadevan and M. Palaniandavar, *Inorg. Chem*., 1998, **37**, 3927-3934.

4 S. Kundu, M. K. Biswas, A. Banerjee, K. Bhadra, G. S. Kumar, M. G. B. Drew, R. Bhadra and P. Ghosh, *RSC Adv*., 2013, **3**, 3054-3061.

5 P. Tamilselvi and M. Palaniandavar, *Inorg. Chim. Acta*, 2002, **337**, 420-428.

6 M. Chauhan, K. Banerjee and F. Arjmand, *Inorg. Chem.*, 2007, **46**, 3072-3082.

7 J. Haribabu, K. Jeyalakshmi, Y. Arun, N. S. P. Bhuvanesh, P. T. Perumal and R. Karvembu, *RSC. Adv.,* 2015, **5**, 46031-46049.

8 G. Z. Chen, X. Z. Huang, J. G. Xu, Z. B. Wang and Z. Z. Zhang, *Method of Fluorescent Analysis*, Science Press, Beijing, 2nd edn, 1990, 123-126.

9 J. N. Miller, *Proc. Anal. Div. Chem. Soc*. 1979, **16**, 203-208.

10 E. A. Brustein, N. S. Vedenkina and M. N. Irkova, *Photochem. Photobiol*., 1973, **18**, 263-279.